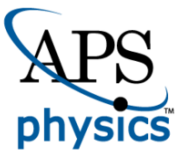

Measurement of inclusive charged current interactions on carbon in a few-GeV neutrino beam

Y. Nakajima *et al.* (SciBooNE Collaboration)

Phys. Rev. D **83**, 012005 — Published 26 January 2011

DOI: 10.1103/PhysRevD.83.012005

Measurement of inclusive charged current interactions on carbon in a few-GeV neutrino beam

Y. Nakajima,[10] J. L. Alcaraz-Aunion,[1] S. J. Brice,[4] L. Bugel,[13] J. Catala-Perez,[18] G. Cheng,[3] J. M. Conrad,[13] Z. Djurcic,[3] U. Dore,[15] D. A. Finley,[4] A. J. Franke,[3] C. Giganti,[15, a] J. J. Gomez-Cadenas,[18] P. Guzowski,[6] A. Hanson,[7] Y. Hayato,[8] K. Hiraide,[10, 8] G. Jover-Manas,[1] G. Karagiorgi,[13] T. Katori,[7, 13] Y. K. Kobayashi,[17] T. Kobilarcik,[4] H. Kubo,[10] Y. Kurimoto,[10, 5] W. C. Louis,[11] P. F. Loverre,[15] L. Ludovici,[15] K. B. M. Mahn,[3, b] C. Mariani,[3] S. Masuike,[17] K. Matsuoka,[10] V. T. McGary,[13] W. Metcalf,[12] G. B. Mills,[11] G. Mitsuka,[9, c] Y. Miyachi,[17, d] S. Mizugashira,[17] C. D. Moore,[4] T. Nakaya,[10] R. Napora,[14] P. Nienaber,[16] D. Orme,[10] M. Otani,[10] A. D. Russell,[4] F. Sanchez,[1] M. H. Shaevitz,[3] T.-A. Shibata,[17] M. Sorel,[18] R. J. Stefanski,[4] H. Takei,[17, e] H.-K. Tanaka,[13, f] M. Tanaka,[5] R. Tayloe,[7] I. J. Taylor,[6, g] R. J. Tesarek,[4] Y. Uchida,[6] R. Van de Water,[11] J. J. Walding,[6, h] M. O. Wascko,[6] H. B. White,[4] M. Yokoyama,[10, i] G. P. Zeller,[4] and E. D. Zimmerman[2]

(SciBooNE Collaboration)

[1] *Institut de Fisica d'Altes Energies, Universitat Autonoma de Barcelona, E-08193 Bellaterra (Barcelona), Spain*
[2] *Department of Physics, University of Colorado, Boulder, Colorado 80309, USA*
[3] *Department of Physics, Columbia University, New York, NY 10027, USA*
[4] *Fermi National Accelerator Laboratory; Batavia, IL 60510, USA*
[5] *High Energy Accelerator Research Organization (KEK), Tsukuba, Ibaraki 305-0801, Japan*
[6] *Department of Physics, Imperial College London, London SW7 2AZ, UK*
[7] *Department of Physics, Indiana University, Bloomington, IN 47405, USA*
[8] *Kamioka Observatory, Institute for Cosmic Ray Research, University of Tokyo, Gifu 506-1205, Japan*
[9] *Research Center for Cosmic Neutrinos, Institute for Cosmic Ray Research, University of Tokyo, Kashiwa, Chiba 277-8582, Japan*
[10] *Department of Physics, Kyoto University, Kyoto 606-8502, Japan*
[11] *Los Alamos National Laboratory; Los Alamos, NM 87545, USA*
[12] *Department of Physics and Astronomy, Louisiana State University, Baton Rouge, LA 70803, USA*
[13] *Department of Physics, Massachusetts Institute of Technology, Cambridge, MA 02139, USA*
[14] *Department of Chemistry and Physics, Purdue University Calumet, Hammond, IN 46323, USA*
[15] *Università di Roma La Sapienza, Dipartimento di Fisica and INFN, I-00185 Rome, Italy*
[16] *Physics Department, Saint Mary's University of Minnesota, Winona, MN 55987, USA*
[17] *Department of Physics, Tokyo Institute of Technology, Tokyo 152-8551, Japan*
[18] *Instituto de Fisica Corpuscular, Universidad de Valencia and CSIC, E-46071 Valencia, Spain*

The SciBooNE Collaboration reports a measurement of inclusive charged current interactions of muon neutrinos on carbon with an average energy of 0.8 GeV using the Fermilab Booster Neutrino Beam. We compare our measurement with two neutrino interaction simulations: NEUT and NUANCE. The charged current interaction rates (product of flux and cross section) are extracted by fitting the muon kinematics, with a precision of 6-15% for the energy dependent and 3% for the energy integrated analyses. We also extract CC inclusive interaction cross sections from the observed rates, with a precision of 10-30% for the energy dependent and 8% for the energy integrated analyses. This is the first measurement of the CC inclusive cross section on carbon around 1 GeV. These results can be used to convert previous SciBooNE cross section ratio measurements to absolute cross section values.

PACS numbers: 13.15.+g, 25.30.Pt

[a] Present address: DSM/Irfu/SPP, CEA Saclay, F-91191 Gif-sur-Yvette, France
[b] Present address: TRIUMF, Vancouver, British Columbia, V6T 2A3, Canada
[c] Present address: Solar-Terrestrial Environment Laboratory, Nagoya University, Furo-cho, Chikusa-ku, Nagoya, Japan
[d] Present address: Department of Physics, Yamagata University, Yamagata, 990-8560 Japan
[e] Present address: Kitasato University, Tokyo, 108-8641 Japan
[f] Present address: Brookhaven National Laboratory, Upton, NY 11973, USA
[g] Present address: Department of Physics and Astronomy, State University of New York, Stony Brook, NY 11794-3800, USA
[h] Present address: Department of Physics, College of William & Mary, Williamsburg, VA 23187, USA
[i] Present address: Department of Physics, University of Tokyo, Tokyo 113-0033, Japan

I. INTRODUCTION

The neutrino charged current (CC) interaction is the process most commonly used to measure neutrino-nucleus scattering in the few-GeV region. It is important for neutrino oscillation measurements because the neutral current (NC) interaction is flavor-blind. However, this interaction mode is poorly understood because of large neutrino flux and cross section uncertainties.

In the energy region above ∼3 GeV, NOMAD [1] and MINOS [2] recently reported precise CC inclusive interaction cross section measurements. However, in the ∼1 GeV region, all inclusive CC measurements have been made on deuterium targets using bubble chambers [3, 4]. In this energy region, the nuclear effects of the neutrino target material (from Fermi motion and the nuclear potential) are significant. Therefore, the cross section on deuterium targets is not directly applicable to the heavier nuclear target materials used in the recent accelerator-based neutrino experiments in this energy region, e.g. SciBooNE, MiniBooNE [5] and T2K [6]. Furthermore, the results in Ref. [4] use CC quasi elastic (QE) interactions to normalize the absolute neutrino flux, which introduces additional ambiguity from the choice of CC-QE interaction model parameters.

Because of the poor knowledge of the cross section, there are multiple neutrino interaction simulators used to predict different cross sections and kinematics of final state particles. Among these, NEUT [7, 8] and NUANCE [9] are commonly used for the recent neutrino oscillation and interaction measurements. NEUT is used in the Kamiokande [10], Super-Kamiokande [11], K2K [12], and T2K experiments, while NUANCE is used in MiniBooNE and as a check of simulations by multiple experiments. They are both tuned to describe the experimental data, however, they have not yet been precisely compared with each other in a single experiment.

In this paper, we report on the comparison of CC candidate events observed in SciBooNE with predictions based on the NEUT and NUANCE neutrino interaction simulators, as well as on the measured CC interaction rate (product of flux and cross section) as a function of neutrino energy extracted from these comparisons. We also report on the first measurement of the CC inclusive interaction cross section on carbon in the 1 GeV region, which is relevant to ongoing and future neutrino oscillation experiments.

In addition to this general purpose, this analysis is also motivated by two direct applications to our measurements. The first is to provide a constraint on the product of flux and cross-section for the forthcoming SciBooNE and MiniBooNE joint ν_μ disappearance analysis [13]. The MiniBooNE collaboration recently performed a search for ν_μ and $\overline{\nu}_\mu$ disappearance using only MiniBooNE data, in which the largest uncertainty stems from the flux and cross section uncertainties [14]. As shown in Fig. 1, the SciBooNE detector is located 440 m upstream of the MiniBooNE detector, sharing the same neutrino beam. In addition, the neutrino target materials are both essentially carbon; polystyrene (C_8H_8) for SciBooNE, and mineral oil (CH_2) for MiniBooNE. Therefore, most of the flux and cross section uncertainties cancel when we compare the data from the two experiments. Then, a ν_μ disappearance search with higher sensitivity becomes possible [13].

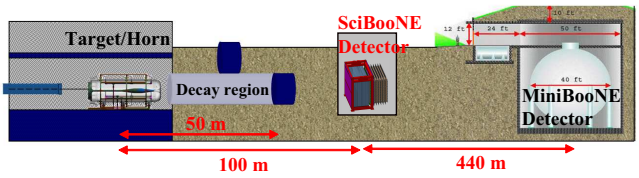

FIG. 1. (color online). Schematic overview of the Booster Neutrino Beamline and the location of the SciBooNE and the MiniBooNE detectors. (not to scale).

The second motivation is to provide an absolute normalization factor for SciBooNE's previous cross section ratio measurements. The SciBooNE collaboration recently measured relative cross sections of charged current coherent pion production [15] and neutral current neutral pion production [16, 17], which were both normalized to CC inclusive interactions. This paper provides an absolute CC interaction cross section with the same definition used in the previous analyses, so that the measured ratios can be converted to absolute cross sections.

The remainder of this paper is organized as follows: Section II summarizes the SciBooNE experiment, including the Booster Neutrino Beamline (BNB) and the SciBooNE detector. The simulation of neutrino interactions with nuclei is described in Section III. Section IV describes the methods used to reconstruct CC interactions and defines the sub-samples used. The analysis of the energy dependent neutrino interaction rate is described in Section V. Finally, the results of the CC interaction rate analysis and the extracted CC absolute cross section are presented in Section VI. The final conclusions are given in Section VII.

II. SCIBOONE EXPERIMENT

A. Neutrino Beam

SciBooNE detected neutrinos produced by the Fermilab BNB. The same BNB beam is also serving the MiniBooNE experiment. The BNB uses protons accelerated to 8 GeV kinetic energy by the Fermilab Booster synchrotron. Beam properties are monitored on a spill-by-spill basis, and at various locations along the BNB line. Transverse and directional alignment of the beam, beam width and angular divergence, beam intensity and losses along the BNB, are measured and used in the data quality selection[15]. Protons strike a 71.1 cm long beryllium target, producing a secondary beam of hadrons, mainly

pions with a small fraction of kaons. A cylindrical horn electromagnet made of aluminum surrounds the beryllium target to sign-select and focus the secondary beam. For the data set used in this measurement, the horn polarity was set to neutrino mode, focusing particles with positive electric charge. The neutrino beam is mostly produced in the 50 m long decay region, mainly from $\pi^+ \to \mu^+\nu_\mu$ in-flight decays.

The analysis presented here uses the full neutrino data set: 0.99×10^{20} protons on target (POT) collected between October 2007 and April 2008.

B. Neutrino Flux Prediction

Predictions for the BNB neutrino flux illuminating the SciBooNE detector are obtained via a GEANT4 [18] simulation of the beamline. Hadronic interactions in the beryllium target are carefully modeled. For π^+ production, a parametrization based on HARP [19] and BNL E910 [20] data are used. The total, inelastic and quasi-elastic hadronic cross sections of protons, neutrons, π^+s and π^-s with Be or Al are treated via custom cross section models [21]. Other hadronic and all electromagnetic processes of importance to neutrino production are described by standard GEANT4 models. For a detailed description of the BNB simulation code, see Ref. [21]. A total neutrino flux per proton on target of 2.2×10^{-8} cm^{-2} is expected at the SciBooNE detector location for the neutrino running mode. The flux is dominated by muon neutrinos (93%).

Figure 2 shows the ν_μ flux from π^+ and K^+ decays, and their fractional uncertainties. The ν_μ energy spectrum peaks at $\sim$ 0.6 GeV, and extends up to 2-3 GeV. The mean energy of the ν_μ flux is expected to be 0.76 GeV. The largest error on the predicted neutrino flux results from the uncertainty of pion production in the initial p-Be process in the target. The simulation predicts that 96.7% of muon neutrinos in the BNB are produced via π^+ decay. The uncertainty in π^+ production is determined from spline fits to the HARP π^+ double differential cross section data [21]. The HARP data used are those from a thin (5% interaction length) beryllium target run [19]. While the HARP data provide a valuable constraint on the BNB flux prediction, additional uncertainties resulting from thick target effects (secondary re-scattering of protons and pions) are included through the BNB flux simulation. The resulting π^+ production uncertainty is $\approx$ 5% at the peak of the flux distribution and increases significantly at high and low neutrino energies.

The flux from K^+ decay is dominant for $E_\nu > 2.3$ GeV. Since no published data exist for K^+ production at the BNB primary proton beam energy, we employ the Feynman scaling hypothesis to relate K^+ production measurements at different proton beam energies to the expected production at the BNB proton beam energy [21]. The errors of the Feynman scaling parameters obtained from these measurements are accounted for in the systematic error. Other major contributions to the flux error include uncertainties on hadron interactions in the target and simulation of the the horn magnetic field, which both contribute to shape and normalization uncertainties, as well as the measurement of the number of POT, which is a pure normalization uncertainty. All flux errors are modeled through variations in the simulation and result in a total error of $\approx$ 7% at the peak of the flux.

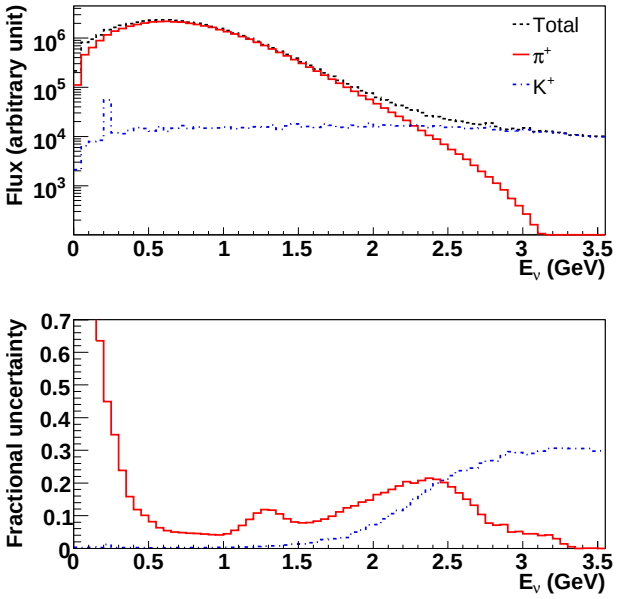

FIG. 2. (color online). (Top) ν_μ flux prediction at the SciBooNE detector as a function of neutrino energy E_ν. The total flux and contributions from π^+ and K^+ decays are shown. (Bottom) Fractional uncertainty of the ν_μ flux prediction due to π^+ and K^+ production from the p-Be interaction. Additional uncertainties from POT, hadron interactions in the target, and the horn magnetic field are not shown.

C. SciBooNE Detector

The SciBooNE detector is located 100 m downstream from the beryllium target on the beam axis, as shown in Fig. 1. The detector comprises three sub-detectors: a fully active and finely segmented scintillator tracker (SciBar), an electromagnetic calorimeter (EC), and a muon range detector (MRD). SciBar is the primary neutrino target for this analysis. In this analysis, we use the data from SciBar and the MRD, and the data from the EC are not used.

SciBooNE uses a right-handed Cartesian coordinate system in which the z axis is the beam direction and the y axis is the vertical upward direction. The origin is located on the most upstream surface of SciBar in the z dimension, and at the center of the SciBar scintillator plane in the x and y dimensions. Since each sub-detector is read out both vertically and horizontally, two views

are defined: top (x vs. z projection) and side (y vs. z projection).

The SciBar detector [22] was positioned upstream of the other sub-detectors. It consists of 14,336 extruded plastic scintillator strips. Each strip has a dimension of $1.3 \times 2.5 \times 300$ cm^3. The scintillators are arranged vertically and horizontally to construct a $3 \times 3 \times 1.7$ m^3 volume with a total mass of 15 tons. The dominant component of the SciBar detector is polystyrene (C_8H_8). We measured the density of the scintillator by sampling 10% of the strips before the installation [23]. The uncertainty of the total detector mass is estimated to be 1%, including the effect of epoxy resin used to glue the strips.

Each strip is read out by a wavelength shifting (WLS) fiber attached to a 64-channel multi-anode photomultiplier (MA-PMT). Charge information is recorded for each channel, while timing information is recorded in groups of 32 channels by taking the logical OR with multi-hit TDC modules [24]. The timing resolution for minimum-ionizing particles, evaluated with cosmic ray data, is 1.6 ns. The average light yield for minimum-ionizing particles is approximately 20 photo-electrons per 1.3 cm path length, and the typical pedestal width is below 0.3 photo-electron. The hit finding efficiency, evaluated with cosmic ray data, is more than 99.8%. The minimum length of a reconstructable track is approximately 8 cm (three layers hit in each view). The track finding efficiency for single tracks of 10 cm or longer is more than 99%.

The MRD is located downstream of SciBar and the EC, and is designed to measure the momentum of muons produced by CC neutrino interactions. It comprises 12 iron plates with thickness 5 cm sandwiched between planes of 6 mm thick scintillation counters; there are 13 alternating horizontal and vertical planes read out via 362 individual 2 inch PMTs. Each iron plate measured 274 $\times$ 305 cm^2. The MRD measures the momentum of muons up to 1.2 GeV/c using the observed muon range. Charge and timing information from each PMT are recorded. The average hit finding efficiency is 99%.

D. Detector Simulation

A GEANT4 framework is used for the detector simulation. The detector simulation includes a detailed geometric model of the detector, including the detector frame and experimental hall and soil.

The Bertini cascade model within GEANT4 [25] is used to simulate the interactions of hadronic particles with detector materials. A 10% difference of the total pion-carbon cross section is seen for higher energy pions between the GEANT4 simulation and external measurements. Hence, we set $\pm$10% systematic uncertainty for the pion-carbon cross section. The systematic uncertainty of the energy deposit per unit length is estimated to be 3% in SciBar and MRD, and 10% in EC, which is dominated by the differences among various calculations of the range to energy conversion. Birk's constant for the SciBar scintillator was measured to be 0.0208 ± 0.0023 cm/MeV [26].

The crosstalk of the MA-PMT is measured to be 3.15$\pm$0.4% for adjacent channels. The single photo-electron resolution of the MA-PMT is set to 50% in the simulation, to reproduce the observed dE/dx distribution of cosmic muons. The absolute error is estimated to be $\pm$20%. A more detailed description of the detector simulation is given in [15].

III. NEUTRINO INTERACTION SIMULATION

A. Overview

We simulate neutrino interactions with carbon and hydrogen in the SciBar detector with the NEUT and NUANCE program libraries. We produced separate Monte Carlo samples with NEUT and NUANCE, and compared the two to the SciBooNE neutrino data.

The nuclear targets handled in NEUT are protons, carbon, oxygen, and iron. The energy of neutrinos handled by the simulation ranges from 100 MeV to 100 TeV. The types of neutrino interactions simulated in both NC and CC are : elastic and quasi-elastic scattering ($\nu N \rightarrow \ell N'$), single meson production ($\nu N \rightarrow \ell N' m$), single gamma production ($\nu N \rightarrow \ell N' \gamma$), coherent π production ($\nu\,^{12}$C(or^{56}Fe) $\rightarrow \ell\pi\,^{12}$C(or^{56}Fe)), and deep inelastic scattering ($\nu N \rightarrow \ell N' hadrons$), where N and N' are the nucleons (proton or neutron), ℓ is the lepton (electron, muon or neutrino), and m is the meson. In nuclei, interactions of the mesons and hadrons with the nuclear medium are simulated following the neutrino interactions.

The types and models of neutrino interactions in NUANCE are similar to those in NEUT but with different cross section parameter settings in some cases and a completely independent treatment of meson and hadron reinteractions in the nuclear medium.

In addition to the neutrino interactions inside SciBar, we also simulate interactions in the EC/MRD and the surrounding materials (the walls of the detector hall and soil) using NEUT. We assign a 20% normalization uncertainty to the interaction cross sections for both the EC/MRD and surrounding material relative to the predictions for SciBar.

B. Neutrino Interaction Model

1. *Quasi-elastic scattering*

The dominant interaction in the SciBooNE neutrino energy range is CC-QE scattering, which is implemented using the Smith and Moniz model [27]. The nucleons are treated as quasi-free particles and the Fermi motion of nucleons along with the Pauli exclusion principle is taken

into account. The Fermi surface momentum (p_F) for carbon is set to 217(220) MeV/c and the nuclear potential (E_B) is set to 25(34) MeV/c in NEUT(NUANCE), as extracted from electron scattering data [28]. The default binding energy in NUANCE is somewhat higher because it additionally accounts for neutrino vs. electron scattering differences [29]. The systematic errors for p_F and E_B are set to $\pm$ 30 MeV/c and $\pm$ 9 MeV/c, respectively, for both NEUT and NUANCE.

For the vector form factor, NEUT uses a dipole form with a vector mass of 0.84 GeV/c^2, while NUANCE uses the BBA-2003 form factor [30]. A dipole form is used for the axial form factor with an adjustable axial mass, M_A^{QE}, for both NEUT and NUANCE. In NUANCE, an empirical Pauli-blocking parameter, κ, is introduced [31] to better describe the MiniBooNE quasi-elastic data at low momentum transfer. When $\kappa > 1$, the phase space of nucleons susceptible to Pauli-blocking is increased and hence the cross section at low momentum transfer is suppressed.

The values of $M_A^{QE} = 1.21$ GeV/c^2 and $\kappa = 1.000$ (i.e. no additional Pauli blocking adjustment) are used in NEUT, and $M_A^{QE} = 1.23$ GeV/c^2 and $\kappa = 1.022$ are used in NUANCE [29]. A systematic uncertainty of $\pm$ 0.22 GeV is assigned to M_A^{QE} to span the difference between the value used and the global fit from previous measurements [32]. The difference between $\kappa = 1.000$ and $\kappa = 1.022$ is also assigned as systematic uncertainty.

The same Fermi momentum distribution, nuclear potential are used in all other neutrino-nucleus interactions except for coherent π production.

2. Meson production via baryon resonances

The second most frequent interaction in SciBooNE is the resonant production of single pion, kaon, and eta mesons as described by the model of Rein and Sehgal (RS) [33].

The RS model assumes an intermediate baryon resonance, N^*, in the reaction of $\nu N \to \ell N^*, N^* \to N'm$. All intermediate baryon resonances with mass less than 2 GeV/c^2 are included. Baryon resonances with mass greater than 2 GeV/c^2 are simulated as deep inelastic scattering. Δ re-interactions ($\Delta N \to NN$) which do not lead to a mesonic final state are also simulated. This re-interaction probability is assumed to be 0.2 $\pm$ 0.2 for all Δ resonances in NEUT and 0.1 $\pm$ 0.1 (0.2 $\pm$ 0.2) for $\Delta^{++/-}$ ($\Delta^{+/0}$) resonances in NUANCE.

To determine the angular distribution of final state pions, the RS method [34] is used for the $P_{33}(1232)$ resonance in both NEUT and NUANCE. For other resonances, the directional distribution of the generated pion is chosen to be isotropic in the resonance rest frame.

The axial-vector form factors are formalized to be dipole with $M_A^{1\pi} = 1.21$ GeV/c^2 for NEUT and $M_A^{1\pi} = 1.10$ GeV/c^2 for NUANCE, with an uncertainty of 0.28 GeV/c^2 in both cases.

An additional uncertainty is assigned to account for the observed Q^2 disagreement between the SciBooNE CC 1π-enriched data samples and NEUT [15]. A similar disagreement is also observed for NUANCE. The size of the uncertainty is determined by re-weighting CC resonant pion events as a function of true Q^2 such that they match the observed distribution in the SciBooNE data, and using the difference between the re-weighted distribution and the central value as the uncertainty.

Resonance decays leading to multi-pion final states are also included in the model and are simulated assuming $M_A^{N\pi} = 1.30 \pm 0.52$ GeV/c^2 in NUANCE. This value of $M_A^{N\pi}$ is chosen strictly to ensure that the total CC cross section prediction reproduces previous experimental data. In NEUT, multi-pion production is simulated as deep inelastic scattering as described later in Sec. III B 4, and the RS model is not used. The size of the systematic uncertainty is estimated based on $M_A^{N\pi}$ variations for NUANCE, and the same size error is assumed also for the NEUT prediction.

3. Coherent pion production

Coherent pion production is a neutrino interaction with a nucleus which remains intact, releasing one pion with the same charge as the incoming weak current. Because of the small momentum transfer to the target nucleus, the outgoing pion tends to be emitted in the forward direction, closely following the incoming neutrino direction. The formalism developed by Rein and Sehgal [35, 36] is used to simulate such interactions. The axial vector mass, M_A^{coh}, is set to 1.0 ± 0.28 GeV/c^2 in both NEUT and NUANCE. In NEUT, the total and inelastic pion-nucleon cross sections from the original Rein-Sehgal publication are employed [35, 36]. In NUANCE, they are obtained from fits to PDG data [37] and implemented as a function of pion energy. Additionally, the NC and CC coherent pion production cross section predictions in NUANCE are rescaled by a factor of 0.65 to better match the measured rate of NC coherent π^0 production as measured in MiniBooNE [38].

4. Deep inelastic scattering

The deep inelastic scattering (DIS) cross section is calculated using the GRV98 parton distribution functions [39]. Additionally, we have included the corrections in the small Q^2 region developed by Bodek and Yang[40] for both NEUT and NUANCE. The implementation of the model is slightly different in NEUT and NUANCE.

In NEUT, the DIS contribution is included for hadronic invariant masses $W > 1.3$ GeV/c^2. The pion multiplicity is additionally restricted to be greater than one for $1.3 < W < 2$ GeV/c^2 to avoid double-counting sources of single pion production that are already included in the resonance portion of the simulation. The

multi-hadron final states are simulated with two models in NEUT: a custom-made program [41] for events with W between 1.3 and 2.0 GeV/c^2 and PYTHIA/JETSET [42] for events with W larger than 2 GeV/c^2.

A restriction on pion multiplicity is not enforced by NUANCE. Instead, the DIS contribution slowly increases for W values starting at 1.7 GeV and becomes the only source of neutrino interactions above $W > 2$ GeV. This is done to create a smooth transition between the resonance and DIS models and ensure continuity in distributions of kinematics and hadron multiplicity in the region of overlap.

TABLE I. Parameters used for neutrino interaction simulation.

Parameter	NEUT	NUANCE
p_F	217 MeV	220 MeV
E_B	25 MeV	34 MeV
M_A^{QE}	1.21 GeV	1.23 GeV
κ	1.00	1.022
$M_A^{1\pi}$	1.21 GeV	1.10 GeV
M_A^{coh}	1.0 GeV	1.0 GeV
$M_A^{N\pi}$	(DIS)	1.3 GeV

5. *Intra-nuclear interactions*

Following production, the intra-nuclear interactions of mesons and nucleons are simulated using a cascade model in which the particles are traced until they escape from the nucleus.

Although we only use kinematic information from the final state muon in this analysis, the simulation of intra-nuclear interactions is important since the pions/protons emitted from the nucleus can be mis-reconstructed as muons.

The inelastic scattering, charge exchange and absorption of pions in nuclei are simulated. For inelastic scattering and charge exchange interactions, the direction and momentum of pions are affected. In the scattering amplitude, Pauli blocking is also taken into account. A more detailed description of the intra-nuclear interaction simulations in NUANCE and NEUT can be found elsewhere [9, 15].

A 25% (30%) uncertainty in the overall pion absorption (charge exchange) cross section is assumed based on comparisons to pion-carbon scattering data [43]. The uncertainty in proton re-scattering is estimated to be 10%. Hence, we apply a 10% error on the number of proton tracks observed in SciBar. Additionally, we set a 20% uncertainty on the NC/CC ratio, estimated from the model dependence of the lepton-mass effect in the small Q^2 region.

C. The Expected Number of Neutrino Events

Table I summarizes the parameter choices used in NEUT and NUANCE for the comparisons presented here. We chose these parameters since they are the default parameter settings used in Super-K, K2K and T2K (NEUT) and MiniBooNE (NUANCE). The different parameter values result in different neutrino cross section predictions between the two.

With the SciBooNE neutrino beam exposure of 0.99×10^{20} protons on target, the expected number of events in the SciBooNE detector for each neutrino interaction is listed in Table II. Because of the difference in parameter choices (Table I), NEUT predicts a larger QE and single pion rate than NUANCE. The difference in QE rate is largely coming from the choice of κ values, and the difference in single pion rate can be largely accounted for by the difference in $M_A^{1\pi}$ assumptions. The major source of the factor of two larger multi-pion/DIS rate in NEUT compared to NUANCE is the difference of multi pion production simulation in the range $1.3 < W < 2.0$ GeV; NEUT simulate these events as DIS, while NUANCE uses a resonant production model. These differences in cross section predictions between similar models with perfectly reasonable parameter choices further highlight the inherent uncertainty in neutrino generator predictions and stress the importance of additional neutrino interaction measurements in this region.

Figure 3 shows the expected number of total ν_μ CC interactions as a function of neutrino energy. One can see that the cross section prediction from NEUT is about 10 - 20% larger than that from NUANCE across the range of SciBooNE energies.

The expected number of ν_μ CC interactions in the 10.6 ton SciBar fiducial volume (Sec. IV B) are 9.11×10^4 and 7.83×10^4 for the NEUT and NUANCE predictions, respectively.

IV. CC EVENT RECONSTRUCTION AND SELECTION

To measure the rate of CC inclusive interactions, we use neutrino events occurring in SciBar with a muon in the final state. We select muons originating in the SciBar fiducial volume (FV), defined to be ± 130 cm in both the x and y dimensions, and $2.62 < z < 157.2$ cm, a total mass of 10.6 tons.

We describe the reconstruction of muon tracks in Sec. IV A, the event selections and details the of subsamples in Sec. IV B and comparison of the data to the MC predictions in Sec. IV C.

TABLE II. The expected number and fraction of events in each neutrino interaction estimated by NEUT and NUANCE at the SciBooNE detector location with the neutrino beam exposure of 0.99×10^{20} protons on target. The 10.6 ton fiducial volume of the SciBar detector is assumed. CC and NC interactions are abbreviated as CC and NC, respectively.

	NEUT		NUANCE	
Interaction Type	# Events	Fraction(%)	# Events	Fraction(%)
CC quasi-elastic	53,038	41.5	47,573	43.6
CC single π via resonances	29,452	23.0	25,863	23.7
CC coherent π	1,760	1.4	1,736	1.6
CC multi-pion, DIS, etc	6,834	5.3	3,140	2.9
NC total	36,836	28.8	30,734	28.2
Total	127,920	100.0	109,046	100.0

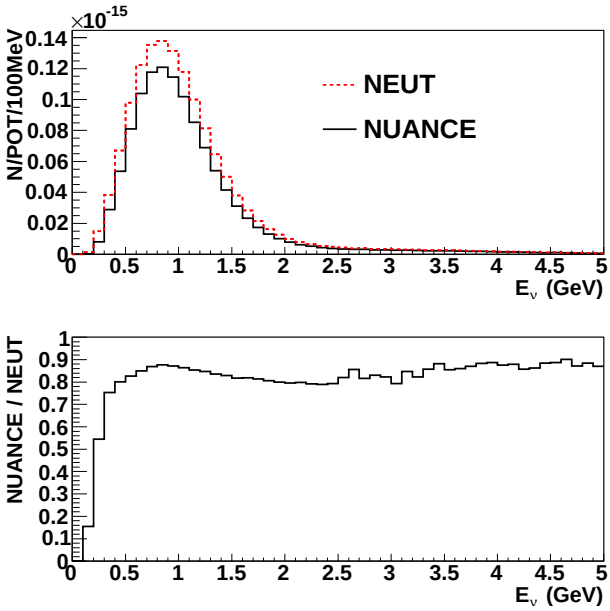

FIG. 3. (color online). The neutrino energy distributions of ν_μ CC interactions at the SciBar detector generated by NEUT (red dashed line) and NUANCE (black solid line). Top plot is the number of interactions per unit POT, and the bottom plot shows the ratio between the NEUT and NUANCE predictions.

A. Track Reconstruction

1. *Track finding*

The first step of the event reconstruction is to search for two-dimensional tracks in each view of SciBar using a cellular automaton algorithm [44]. Three dimensional tracks are reconstructed by matching the timing and z-edges of the two dimensional projections; differences between two two-dimensional projections are required to be less than 50 ns, and the z-edge difference must be less than 6.6 cm for both upstream and downstream edges. The two dimensional tracks in MRD are independently reconstructed using hits in the MRD clustered within a 50 ns timing window. Three dimensional tracks in the MRD are reconstructed by matching the timing of the two dimensional projections.

Then, if the downstream edge of a SciBar track lies in last two layers of SciBar, we search for a track or hits in the MRD that are matched with the SciBar track. For matching an MRD track to a SciBar track, the upstream edge of the MRD track is required to be on either one of the first two layers of the MRD, and to be within 30 cm of the projected entry point of the SciBar track into the MRD in each view. A SciBar track matched with MRD is defined as a SciBar-MRD matched track. The matching criteria impose a muon momentum threshold of 350 MeV/c. A more detailed description of the track reconstruction can be found elsewhere[15].

2. *Track Classification*

We define three types of tracks used in this analysis: SciBar-stopped, MRD-stopped and MRD-penetrated tracks, as shown in Fig. 4.

Tracks with both edges contained in the SciBar FV are classified as SciBar-stopped tracks. MRD-stopped and MRD-penetrated tracks are both subsets of the SciBar-MRD matched sample. An MRD-stopped track is selected by requiring the downstream edge of the track to be within $|x| < 132$ cm , $|y| < 111$ cm , and $z <$ (last layer of the MRD). An MRD-penetrated track is selected by requiring additional hits at the most downstream scintillator of the MRD. Tracks which exit from the side of the MRD are not used in this analysis.

3. *Particle Identification*

The SciBar detector has the capability to distinguish protons from other particles using dE/dx. We define a muon confidence level (MuCL) using the observed energy

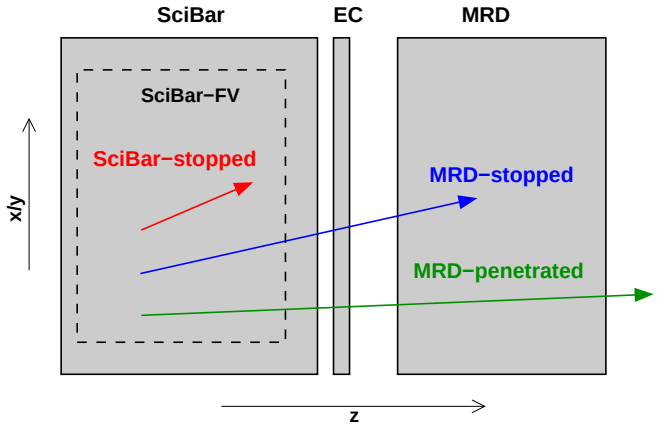

FIG. 4. (color online). Types of tracks used for this CC interaction measurement.

deposit per layer for all reconstructed tracks [15]. Tracks with MuCL greater than 0.05 are considered muon-like (or pion-like) and the others are classified as proton-like.

4. *Muon Kinematics Reconstruction*

The slopes of the muon angles with respect to the beam in the two SciBar views are used to calculate the three dimensional muon angle with respect to the beam (θ_μ).

According to the MC simulation, about 30 % of SciBar-stopped tracks are expected to be backward-going. To identify these backward-going tracks, we use the delayed timing signal produced by the decay electrons from stopped muons. A track is identified to be backward-going if it has (1) at least one delayed hit at $t > 200$ nsec at the upstream ends of the two dimensional views, and (2) no delayed hit at $t > 200$ nsec at the downstream ends. We impose this requirement for both top- and side- PMT signals from the track endpoints to remove hits due to random noise and after pulsing from the PMTs. The performance of this identification is estimated using a MC sample of CCQE events with 1 reconstructed track. In this sample, the efficiency of selecting backward-going tracks is $\sim$ 57%, and the probability of mis-reconstructing a forward track as backward is $\sim$1%. The loss of efficiency is predominantly due to decay electrons emitted at a large angle, producing hits in either the top or side PMTs, but not both.

This track direction identification is only applied to SciBar-stopped tracks. All tracks reaching the MRD are assumed to be forward-going, because the fraction of backward tracks is estimated to be small ($\sim$ 4%) and also a similar tagging of decay electrons is not possible in the MRD since the electrons stop and are undetected within the steel plates.

The kinetic energy of the muon (E_{kin}) is calculated by the range and the expected energy deposition per unit length (dE/dx) in the detector materials

$$E_{kin} = E^{SciBar} + E^{EC} + E^{Wall} + E^{MRD}, \qquad (1)$$

where E^{SciBar}, E^{EC}, E^{Wall} and E^{MRD} are the expected energy deposit by muons in SciBar, the EC, the wall of the dark box between the EC and MRD, and the MRD, respectively.

For SciBar-stopped tracks, E^{EC}, E^{Wall} and E^{MRD} are set to 0, and E^{SciBar} is calculated by a range to energy look-up table based on the MC simulation.

For MRD-stopped tracks, energy deposits in SciBar, EC and the wall are computed as $E^{SciBar} = 2.04$ MeV/cm $\times L_{SB}$ (cm), $E^{EC} = 90.8/\cos\theta_\mu$ MeV and $E^{Wall} = 3.3/\cos\theta_\mu$ MeV, where L_{SB} is the reconstructed track length in SciBar. E^{MRD} is calculated by a range to energy look-up table based on the MC simulation.

The average muon angular resolution is 0.9° for all samples. The muon momentum resolutions are 15 MeV/c for SciBar-stopped and 50 MeV/c for MRD-stopped tracks, respectively.

B. Event Selection and Classification

1. *Event Selection*

We select the highest momentum track with MuCL > 0.05 in an event as a muon candidate. We also require the reconstructed momentum to be greater than 0.25 GeV/c to reject short proton or pion tracks from neutral current interactions. Then, we require the upstream edge of the muon candidate to be in the SciBar FV.

2. *Event Classification*

Events with muon track candidates are subdivided into three sub-samples: SciBar-stopped, MRD-stopped and MRD-penetrated samples, according to the track classification given in Sec. IV A 2 for the muon candidate.

a. SciBar-stopped sample The SciBar-stopped sample provides the lowest energy sample; the mean energy of neutrinos in this sample is 1.0 GeV. According to the simulation, the purity of ν_μ CC interactions in this sample is 85%. Impurities are due to ν_μ NC interactions ($\sim$ 7%), interactions occurring in the surrounding material ($\sim$ 5%) and $\overline{\nu}_\mu$ CC interactions ($\sim$ 1.5%). Figure 5 shows the distributions of the reconstructed muon momentum (p_μ) and angle (θ_μ) for SciBar-stopped muons. The backward-going muon identification described in Sec. IV A 4 is used for this sample. All tracks which are not identified as backward-going are accounted as forward-going tracks for both data and MC samples. The expected number of events in each interaction mode is summarized in Table III. The contamination of the cosmic-ray backgrounds is estimated,

using off-beam data, to be 671.2 ± 11.6 events, where the uncertainty comes from the statistics of the off-beam data sample. This rather large contamination ($\sim 5\%$) is due to cosmic-rays penetrate SciBar vertically, which leave sparse hits and are often mis-reconstructed as short tracks. This effect is negligible for the other sub-samples.

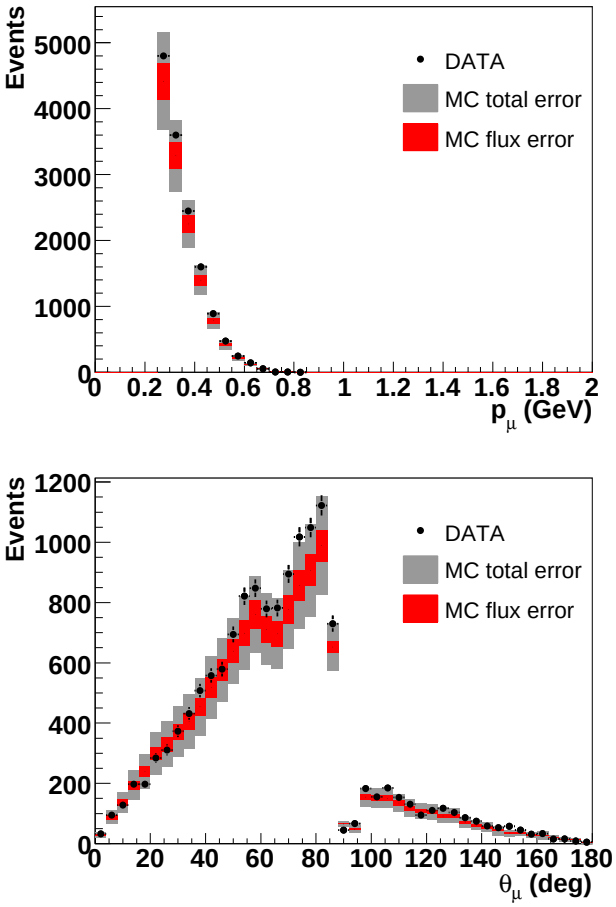

FIG. 5. (color online). Distributions of reconstructed momentum (top) and angle (bottom) of the muon candidate in the SciBar-stopped sample. The MC prediction is based on NEUT and absolutely normalized by the number of POT. The total and flux systematic errors on the MC predictions are separately shown. The dominant source of the total error is the cross section uncertainty.

b. MRD-stopped sample The MRD-stopped sample has the largest statistics among the three. The mean energy of neutrinos in the MRD-stopped sample is 1.2 GeV. According to the simulation, the purity of ν_μ CC interaction in this sample is 91%. Impurities are from neutrino interactions in the EC/MRD which back-scatter ($\sim 4\%$), ν_μ NC interactions ($\sim 3\%$) and $\overline{\nu}_\mu$ CC interactions ($\sim 2\%$). Figure 6 shows the distributions of the reconstructed muon momentum (p_μ) and angle (θ_μ) for MRD-stopped muons. The expected number of events in each interaction mode is summarized in Table IV. The contamination of the cosmic-ray backgrounds is estimated to be 54.6 ± 3.3 events.

TABLE III. The expected number and fraction of events in each neutrino interaction type for the SciBar-stopped sample, as estimated by NEUT and NUANCE. The external events comprise interactions in the EC, MRD and surrounding material.

Interaction	NEUT		NUANCE	
type	Events	Fraction(%)	Events	Fraction(%)
CC QE	5818	47.4	5511	50.8
CC res. 1π	3694	30.1	3226	29.8
CC coh. 1π	119	1.0	123	1.1
CC other	914	7.4	350	3.2
NC	916	7.4	842	7.8
All non-ν_μ	188	1.5	161	1.5
External	629	5.1	629	5.8
Total	12278		10,842	

TABLE IV. The expected number and fraction of events in each neutrino interaction type for the MRD-stopped sample, as estimated by NEUT and NUANCE. The external events comprise interactions in the EC, MRD and surrounding material.

Interaction	NEUT		NUANCE	
type	Events	Fraction(%)	Events	Fraction(%)
CC QE	10341	56.1	8385	52.3
CC res. 1π	4789	26.0	4839	30.2
CC coh. 1π	659	3.6	633	3.9
CC other	1010	5.5	600	3.7
NC	577	3.1	569	3.5
All non-ν_μ	320	1.7	281	1.8
External	729	4.0	729	4.5
Total	18,427		16,036	

c. MRD-penetrated sample The MRD-penetrated sample is the highest energy sample among the three. The mean energy of neutrinos is 2.4 GeV. Although the track angles can be measured, we do not have the capability to reconstruct the muon momentum for the tracks which exit the MRD. However, this sample can provide the normalization for the highest energy region. Hence, this sample is also used for the neutrino interaction rate measurement. According to the simulation, the purity of ν_μ CC interaction in this sample is 97%. Impurities mostly come from $\overline{\nu}_\mu$ CC interactions ($\sim 2\%$). Figure 7 shows the distributions of the reconstructed muon angle (θ_μ) of the MRD-penetrated muons. The expected number of events in each interaction mode is summarized in Table V. The contamination of the cosmic-ray backgrounds is estimated to be 16.6 ± 1.8 events.

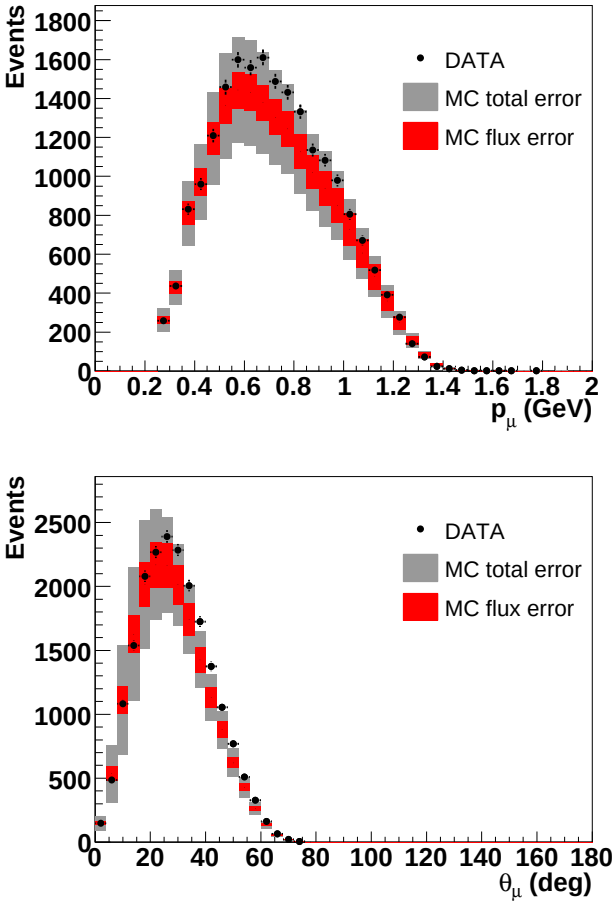

FIG. 6. (color online). Distributions of reconstructed momentum (top) and angle (bottom) of the muon candidate in the MRD-stopped sample. The MC prediction is based on NEUT and absolutely normalized by the number of POT. The total and flux systematic errors on the MC predictions are separately shown. The dominant source of the total error is the cross section uncertainty.

TABLE V. The expected number and fraction of events in each neutrino interaction type for the MRD-penetrated sample, as estimated by NEUT and NUANCE. The external events comprise interactions in the EC, MRD and surrounding material.

Interaction	NEUT		NUANCE	
type	Events	Fraction(%)	Events	Fraction(%)
CC QE	2428	60.0	1943	57.0
CC res. 1π	1008	24.9	976	28.6
CC coh. 1π	140	3.5	130	3.8
CC other	356	8.8	255	7.4
NC	1.5	0.04	2.3	0.07
All non-ν_μ	89	2.2	75	2.2
External	27	0. 7	27	0.8
Total	4049		3407	

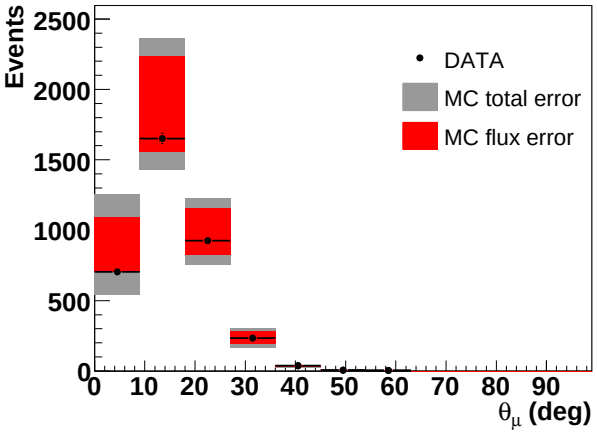

FIG. 7. (color online). Distribution of reconstructed angle of the muon candidate in the MRD-penetrated sample. The MC prediction is based on NEUT and absolutely normalized by the number of POT. The total and flux systematic errors on the MC predictions are separately shown.

3. *Efficiency Summary*

Figure 8 shows the efficiency of CC events as a function of true neutrino energy for each sub-sample, estimated from the NEUT based MC simulation. By combining these three samples, we can obtain fairly uniform acceptance for neutrinos above 0.4 GeV.

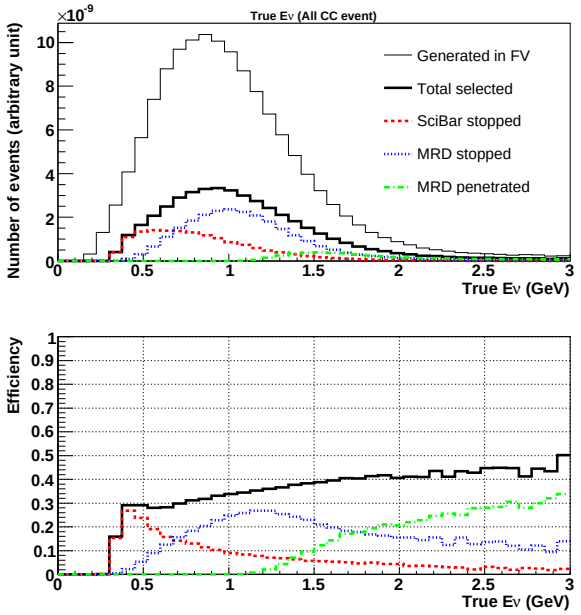

FIG. 8. (color online). (Top) Number of CC events in the SciBar FV as a function of true E_ν, predicted by the NEUT based simulation. The number of selected events in each sub-sample are also shown. (Bottom) Detection efficiency as a function of true neutrino energy for each sub-sample.

C. Data Comparison to the MC prediction

Table VI shows the number of events obtained from data and the predictions from NEUT and NUANCE based MC simulations. The contamination of cosmic-ray backgrounds is estimated using the off-beam data, and have been subtracted from the data. For the total number of events from the three sub-samples, we find a data/MC normalization factor of 1.08 for the NEUT prediction, and 1.23 for the NUANCE prediction.

To compare the MC predictions with data, the neutrino energy(E_ν) and the square of the four-momentum transfer(Q^2) are the key variables since a flux variation is purely a function of E_ν while a variation of the cross section model typically changes the Q^2 distribution. We reconstruct these variables assuming CC-QE interaction kinematics. The reconstructed E_ν is calculated as

$$E_\nu^{rec} = \frac{m_p^2 - (m_n - E_B)^2 - m_\mu^2 + 2(m_n - E_B)E_\mu}{2(m_n - E_B - E_\mu + p_\mu \cos\theta_\mu)}, \quad (2)$$

where m_p, m_n and m_μ are the mass of proton, neutron and muon, respectively, E_μ is the muon total energy, and E_B is the nuclear potential energy. The reconstructed Q^2 is given by,

$$Q^2_{rec} = 2E_\nu^{rec}(E_\mu - p_\mu \cos\theta_\mu) - m_\mu^2. \quad (3)$$

Figure 9 shows the distributions of E_ν^{rec} and Q^2_{rec} for the SciBar-stopped and MRD-stopped samples. In these plots, data points are compared with the NEUT and NUANCE based MC predictions. We find that the data are consistent with the MC predictions within the systematic uncertainties.

V. CC INTERACTION RATE ANALYSIS

A. Method

To calculate the CC inclusive interaction rate and cross section versus energy, we re-weight the predictions of NEUT or NUANCE based simulations in true energy bins by factors that are found to give the best agreement with the kinematic distributions for data versus MC prediction.

The p_μ vs. θ_μ (p_μ-θ_μ) distributions from the SciBar-stopped and the MRD-stopped samples, and θ_μ distribution from the MRD-penetrated sample are simultaneously used for this measurement. Figure 10 shows the p_μ-θ_μ distributions of the SciBar-stopped and MRD-stopped samples, while the θ_μ distribution for the MRD-penetrated sample is shown in Fig. 7. Events in the same p_μ-θ_μ bins but in different sub-samples are not summed together, but treated as separate p_μ-θ_μ bins in the analysis, and only bins with at least 5 entries are used for the fit. The total number of p_μ-θ_μ bins is 159; 71 from the SciBar-stopped, 82 from the MRD-stopped and 6 from the MRD-penetrated samples.

We define 6 rate normalization factors $(f_0, \cdots, f_5)$ which represent the CC interaction rate normalized to the MC prediction for each true energy region defined in Table VII. The events at $E_\nu < 0.25$ GeV are not used since these events are below our detection efficiency as shown in Fig. 8, and also the fraction of these low energy interactions are negligibly small ($< 1\%$) at the BNB flux. We calculate these rate normalization factors by comparing the MC predictions to the measured CC interaction rate. For each energy region, we generate the MC templates for the p_μ-θ_μ distributions in each event sample; n_{ij}^{pred} is the predicted number of events in the j-th p_μ-θ_μ bin, corresponding to energy bin i. The expected number of events in each p_μ-θ_μ bin, N_j^{pred}, is calculated as

$$N_j^{pred} = \sum_i^{E_\nu bins} f_i n_{ij}^{pred}. \quad (4)$$

Figures 11 and 12 are MC templates of the p_μ-θ_μ distributions for the SciBar-stopped and MRD-stopped samples. We see that there is a large contribution in the SciBar-stopped sample of events with E_ν below 0.75 GeV. Hence, this sample is essential to determine the rate normalization factors in the low energy regions. The p_μ-θ_μ distributions of the MRD-stopped sample clearly depends on E_ν, up to 1.75 GeV. However, most of the events in the MRD-stopped sample with $E_\nu > 1.75$ GeV have small reconstructed p_μ. These are events with energetic pion or proton tracks that are mis-reconstructed as muons. Due to the weak constraint from the MRD-stopped sample on events with $E_\nu > 1.75$ GeV, the MRD-penetrated sample is included in the fit since about 2/3 of the events in this sample have $E_\nu > 1.75$ GeV as shown in Fig. 13.

We find the rate normalization factors $(f_0, \cdots, f_5)$ which minimize the χ^2 value defined as:

$$\chi^2 = \sum_{j,k}^{Nbins} (N_j^{obs} - N_j^{pred})(V_{sys} + V_{stat})^{-1}_{jk}(N_k^{obs} - N_k^{pred}). \quad (5)$$

Here, $N_{j(k)}^{obs}$ and $N_{j(k)}^{pred}$ are the observed and predicted numbers of events in the j(k)-th p_μ-θ_μ bin, and $N_{j(k)}^{pred}$ is a function of the rate normalization factors as shown in Eq. (4). V_{sys} is the covariance matrix for systematic uncertainties in each p_μ-θ_μ bin, and V_{stat} represents the statistical error. We have a total of 159 bins, so V_{sys} and V_{stat} are 159×159 dimensional matrices. The details of evaluating V_{sys} are described in the following section.

B. Systematic Errors

The sources of systematic error are divided into four categories: neutrino beam (i), neutrino interaction models (ii), intra-nuclear interaction model (iii), and detector response and neutrino interaction models outside of

TABLE VI. The number of events in each sub-sample from the data and the predictions from NEUT/NUANCE-based MC. The numbers in parentheses show the ratio between the data and the predictions. The cosmic-ray backgrounds are estimated from off-timing data and subtracted from the data.

Sample	SciBar-stopped	MRD-stopped	MRD-penetrated	Total
Data	13588.8	20236.4	3544.4	37369.6
NEUT	12278.3(1.11)	18426.3(1.10)	4049.0(0.88)	34753.6(1.08)
NUANCE	10841.9(1.25)	16036.2(1.26)	3407.5(1.04)	30285.6(1.23)

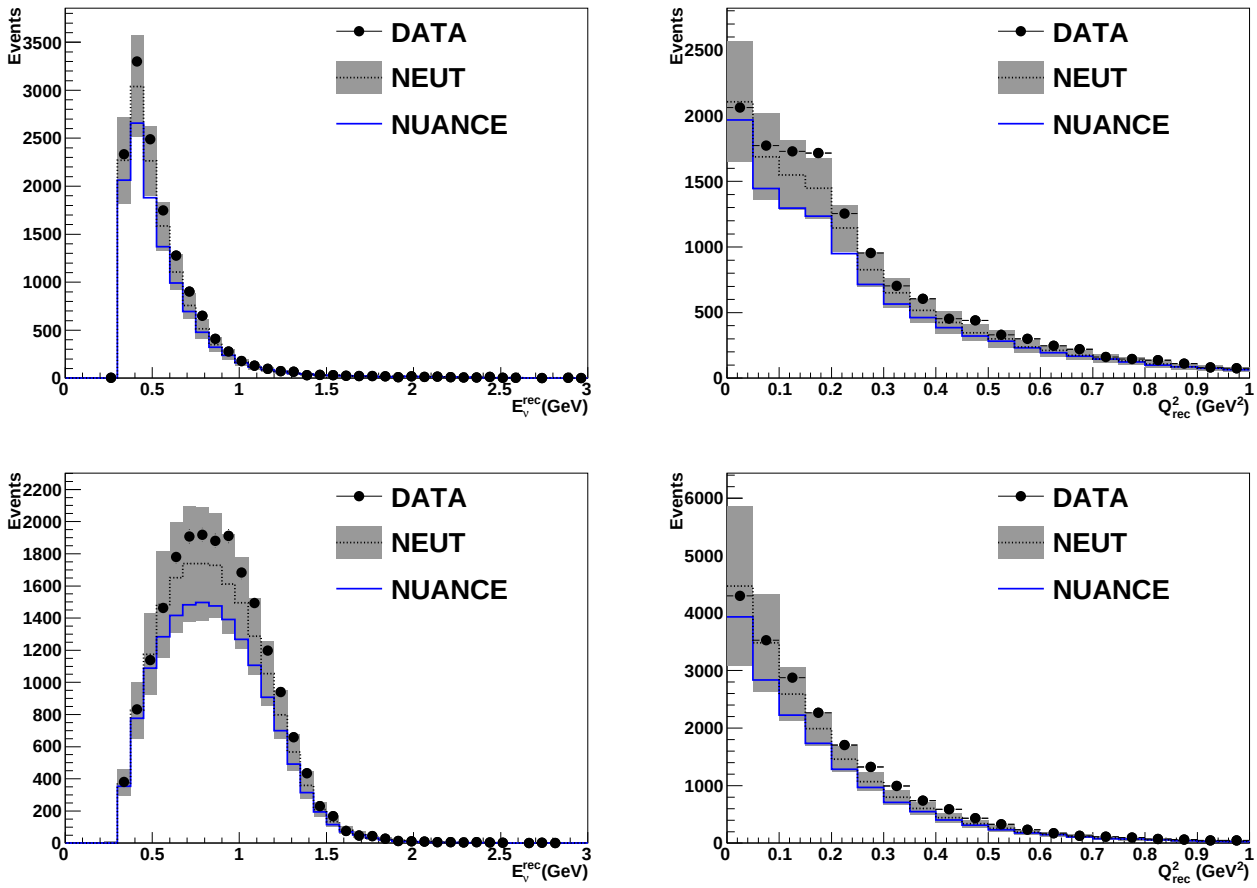

FIG. 9. (color online). Top: E_ν^{rec} (left) and Q^2_{rec} (right) of the SciBar-stopped sample. Bottom: E_ν^{rec} (left) and Q^2_{rec} (right) of the MRD-stopped sample. The NEUT and NUANCE predictions are absolutely normalized by the number of POT. The filled regions show the systematic uncertainties on the MC predictions based on NEUT. The systematic uncertainty for the NUANCE prediction is similar to that of the NEUT prediction and not shown.

SciBar (iv). Table VIII shows the list of the systematic uncertainties considered in this analysis, which were described in the previous sections.

The aim of this fit is to constrain the variations due to flux (i) and cross section (ii) by measuring the rate normalization factors as a function of E_ν, f_i. Uncertainties from (i) and (ii) are factorized into two parts: variations which change the rate normalization of CC events in each E_ν region ("normalization") and variations which change the p_μ-θ_μ distributions but not the normalization of CC events ("p_μ-θ_μ shape"). The former, normalization, is corrected by the use of f_i, so V_{sys} corresponds only to p_μ-θ_μ shape uncertainties for flux and cross section.

The p_μ-θ_μ shape uncertainties are estimated by renormalizing the variation for each E_ν region as follows. First, we generate a new prediction corresponding to a single systematic variation, n'_{ij}. Here, the prime denotes a systematic variation, with i and j representing as before the energy bin i and p_μ-θ_μ bin j.

Then, the predicted event rate, N'_j, corresponding to

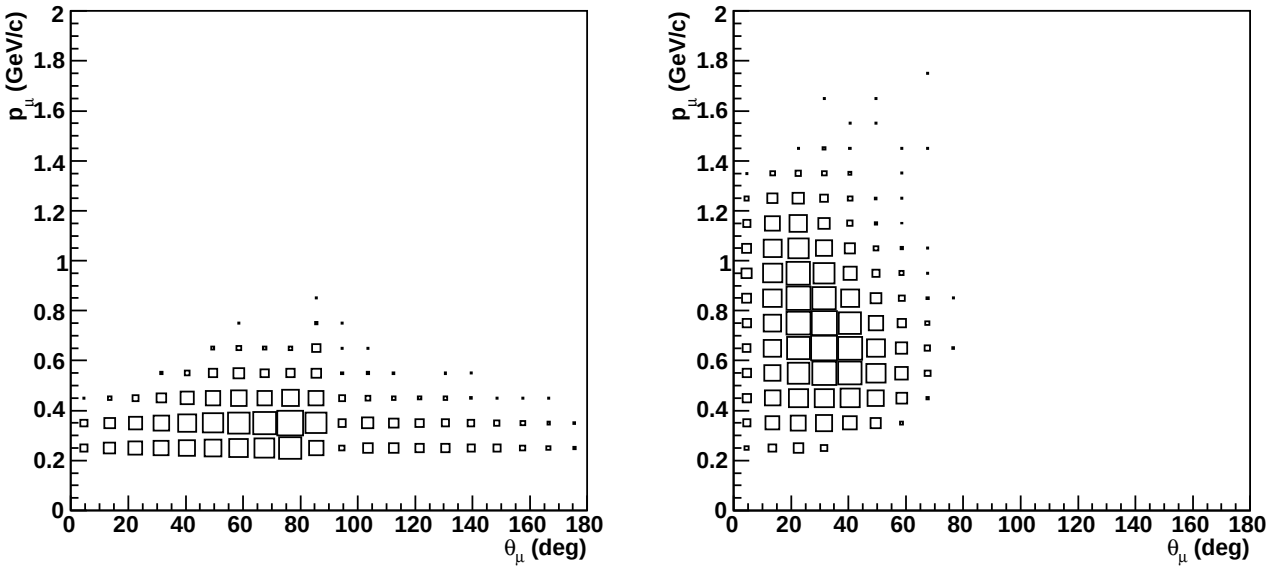

FIG. 10. Data distributions of p_μ vs. θ_μ for the SciBar-stopped (left) and MRD-stopped (right) samples. The size of boxes is proportional to the number of entries.

TABLE VII. Energy regions for the CC interaction rate measurement. These energy regions are in terms of the true neutrino energy from the MC.

Parameter	f_0	f_1	f_2	f_3	f_4	f_5
E_ν range (GeV)	0.25 - 0.5	0.5 - 0.75	0.75 - 1.0	1.0 - 1.25	1.25 - 1.75	1.75+

this systematic variation is:

$$N'_j = \sum_i^{E_\nu bins} f_i n'_{ij} R_i, \tag{6}$$

where R_i is the renormalization factor, which is the ratio of the total number of predicted events in each E_ν bin between central value and systematically varied predictions, defined as:

$$R_i = \frac{\sum_j^{(p_\mu,\theta_\mu)bins} n_{ij}}{\sum_j^{(p_\mu,\theta_\mu)bins} n'_{ij}}. \tag{7}$$

The predictions for central value N_j and n_{ij} are the same as the N_j^{pred} and n_{ij}^{pred} used in Eq. (4).

Unlike the flux and cross section uncertainties, intranuclear interaction (iii) and detector uncertainties (iv) are independent of the CC interaction rate. For these sources, the uncertainties are simply calculated as:

$$N'_j = \sum_i^{E_\nu bins} f_i n'_{ij}. \tag{8}$$

To generate the V_{sys} matrix, the systematically varied rate, N'_{ij}, is compared to the central value event rate. To better estimate some uncertainties, many variation predictions ("draws") are used, each corresponding to a unique set of underlying parameters. To estimate the error from the M_A uncertainty, for example, we generate 1000 different sets of MC expectations of n'_{ij}, each corresponding to the different value of M_A randomly drawn from the estimated uncertainty of M_A. Then, the error matrix representing the uncertainty from M_A is calculated as:

$$V_{jk}^{M_A} = \frac{1}{M}\sum_l^M (N'_{jl} - N_j)(N'_{kl} - N_k), \tag{9}$$

where k denotes the index of random draws and M denotes the total number of draws. We estimate the errors from each source (i) - (iv) individually, then add the matrices together to generate a total covariance matrix, V_{sys}. We assume the same size fractional error for both NEUT and NUANCE based predictions, and the total covariance matrices for them are calculated by scaling the fractional errors with the predictions.

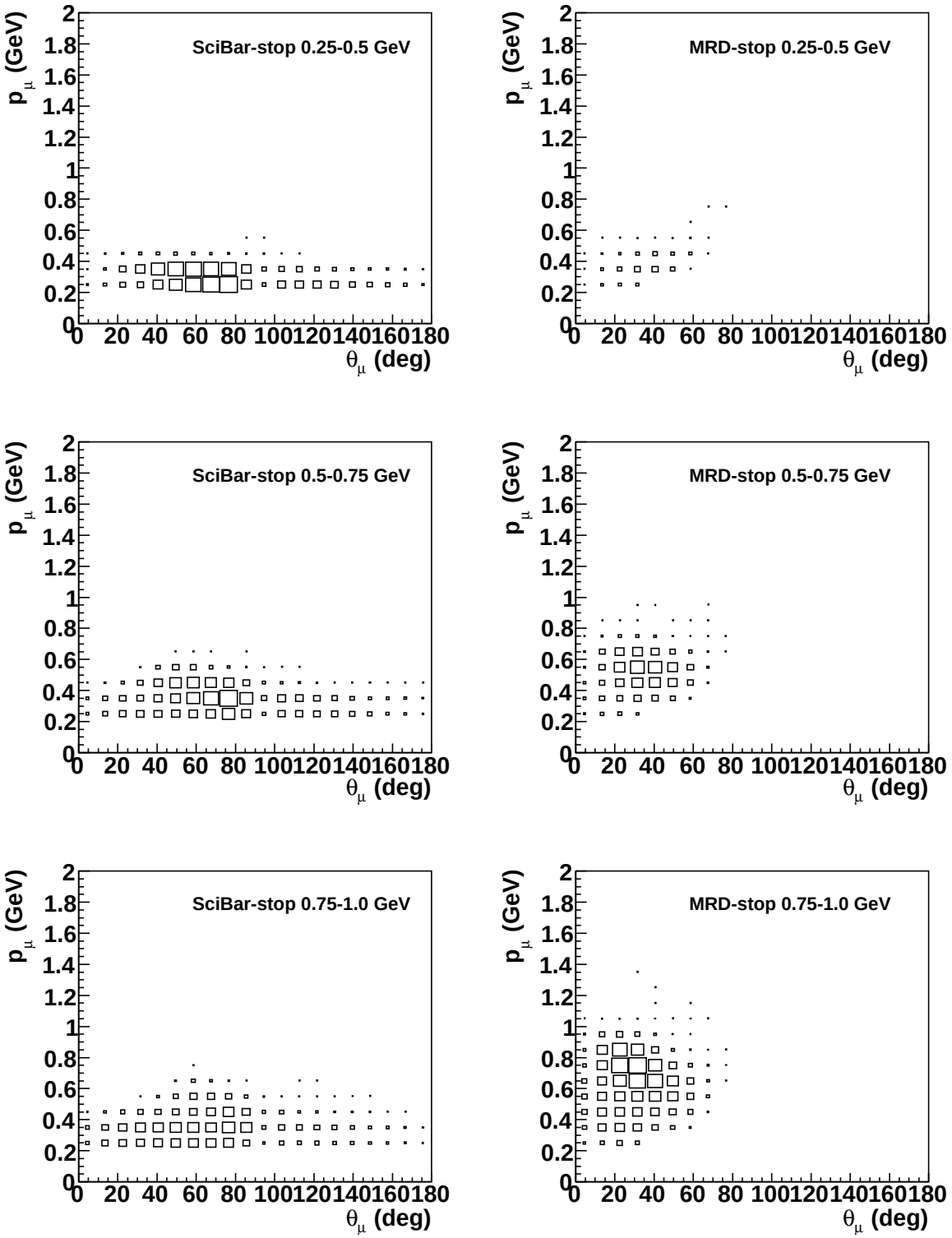

FIG. 11. The MC templates of p_μ vs. θ_μ for the SciBar-stopped and MRD-stopped sample for the three lowest E_ν regions. The normalization factors are common between the SciBar-stopped and MRD-stopped samples.

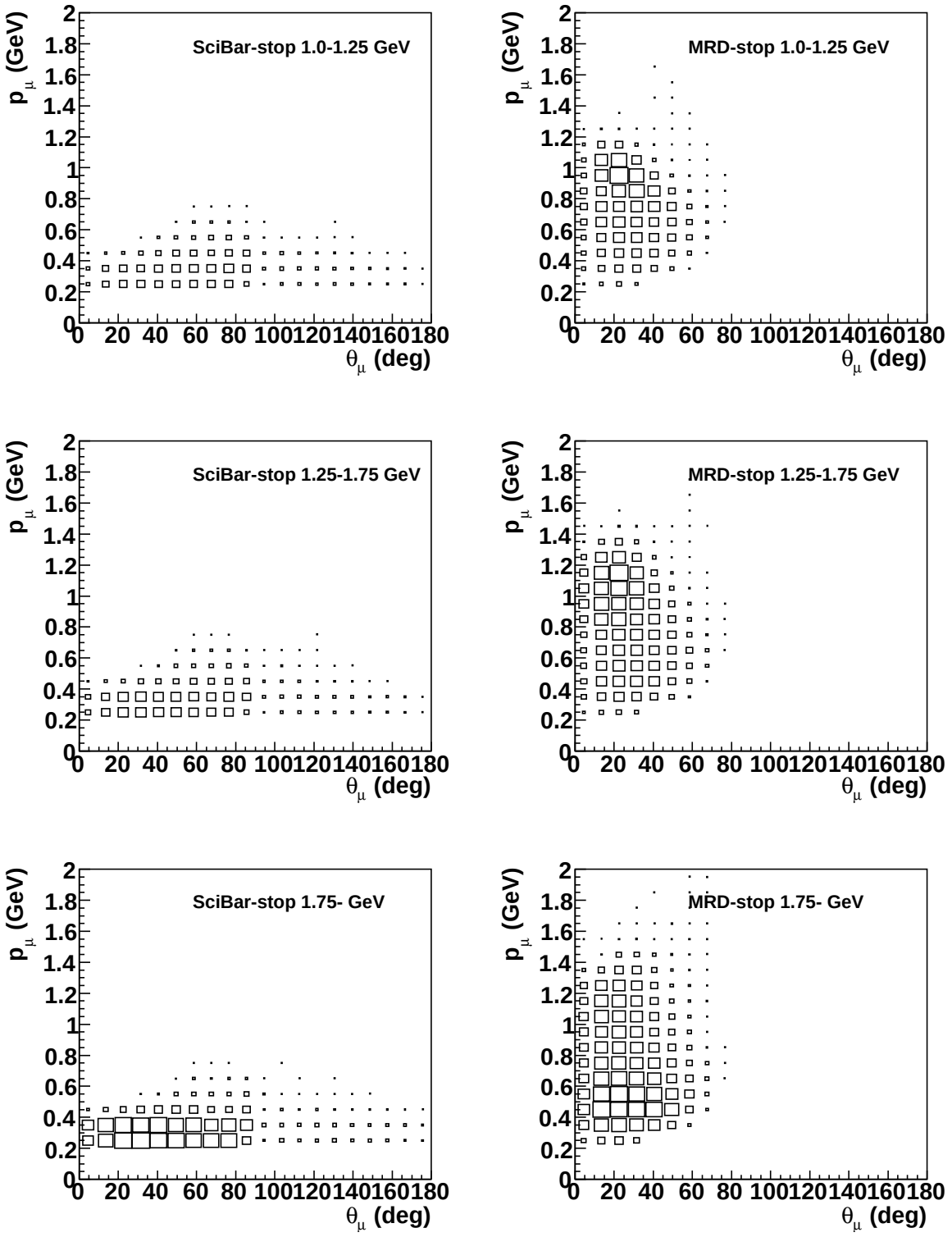

FIG. 12. The MC templates of p_μ vs. θ_μ for the SciBar-stopped and MRD-stopped sample for the three highest E_ν regions. The normalization factors are common between the SciBar-stopped and MRD-stopped samples.

TABLE VIII. List of systematic uncertainties considered.

Category	Error Source	Variation	Description
(i) Flux	π^+/π^- production from p-Be interaction	Spline fit to HARP data [19]	Sec. II B
	K^+/K^0 production from p-Be interaction	Tables VIII and IX in Ref. [21]	Sec. II B
	Nucleon and pion interaction in Be/Al	Table XIII in Ref. [21]	Sec. II B
	Horn current	±1 kA	Sec. II B
	Horn skin effect	Horn skin depth, ±1.4 mm	Sec. II B
	Number of POT	±2%	Sec. II B
(ii) Neutrino interaction	Fermi surface momentum of carbon nucleus	±30 MeV	Sec. III B 1
	Binding energy of carbon nucleus	±9 MeV	Sec. III B 1
	CC-QE M_A	±0.22 GeV	Sec. III B 1
	CC-QE κ	±0.022	Sec. III B 1
	CC-1π M_A	±0.28 GeV	Sec. III B 2
	CC-1π Q^2 shape	Estimated from SciBooNE data	Sec. III B 2
	CC-coherent-π M_A	±0.28 GeV	Sec. III B 3
	CC-multi-π M_A	±0.52 GeV	Sec. III B 4
(iii) Intra-nuclear interaction	Δ re-interaction in nucleus	±100 %	Sec. III B 2
	Pion charge exchange in nucleus	±20 %	Sec. III B 5
	Pion absorption in nucleus	±35 %	Sec. III B 5
	Proton re-scattering in nucleus	±10 %	Sec. III B 5
	NC/CC ratio	±20 %	Sec. III B 5
(iv) Detector response	PMT 1 p.e. resolution	±0.20	Sec. II D
	Birk's constant	±0.0023 cm/MeV	Sec. II D
	PMT cross-talk	±0.004	Sec. II D
	Pion interaction cross section in the detector material	±10 %	Sec. II D
	dE/dx uncertainty	±3%(SciBar,MRD), ±10%(EC)	Sec. II D
	Density of SciBar	±1 %	Sec. II C
	Normalization of interaction rate at the EC/MRD	±20 %	Sec. III A
	Normalization of interaction rate at the surrounding materials	±20 %	Sec. III A
	Contamination of cosmic-ray backgrounds	Estimated from off-beam data	Sec. IV B 2

VI. RESULTS AND DISCUSSION

A. Energy Dependent CC Interaction Rate

1. *Measurement of CC Interaction Rate*

Tables IX and X show the best fit parameters and their errors from the spectrum fit with the six energy dependent rate normalization factors for NEUT and NUANCE predictions, respectively. The χ^2/DOF, where DOF is the number of degree of freedom for NEUT and NUANCE predictions are respectively 225.1/159 and 560.7/159 before fitting, and they are 161.2/153 and 173.6/153 after fitting. We obtain reasonable χ^2 values after the fit. We also tried to tune Q^2 distributions by fitting cross section parameters such as M_A and κ, however, these give similar χ^2 values. So we decided to make fits with simple factors for true E_ν regions, as described above, because they are less model dependent.

Figure 14 shows the distributions of p_μ, θ_μ E_ν^{rec} and Q^2_{rec} of the MRD-stopped sample, after applying the rate normalization factors obtained in this analysis. We estimate the constrained systematic error for each distribution in the same way as described in the Sec. V B. We also propagate the errors of the scale factors (f_i) to the dis-

TABLE IX. Spectrum fit result for the NEUT prediction. The first two rows are the best fit values and associated uncertainties. The subsequent columns and rows represent the correlation coefficients for each parameters.

	f_0	f_1	f_2	f_3	f_4	f_5
Best fit	1.042	1.032	1.234	1.290	1.193	0.789
Error	0.186	0.095	0.064	0.084	0.104	0.083
f_0	1.0000	0.2951	0.1653	-0.2224	-0.3646	0.0438
f_1	0.2951	1.0000	0.0591	-0.3674	-0.5311	-0.2187
f_2	0.1653	0.0591	1.0000	-0.2317	-0.1511	-0.3301
f_3	-0.2224	-0.3674	-0.2317	1.0000	-0.0011	0.2534
f_4	-0.3646	-0.5311	-0.1511	-0.0011	1.0000	-0.0680
f_5	0.0438	-0.2187	-0.3301	0.2534	-0.0680	1.0000

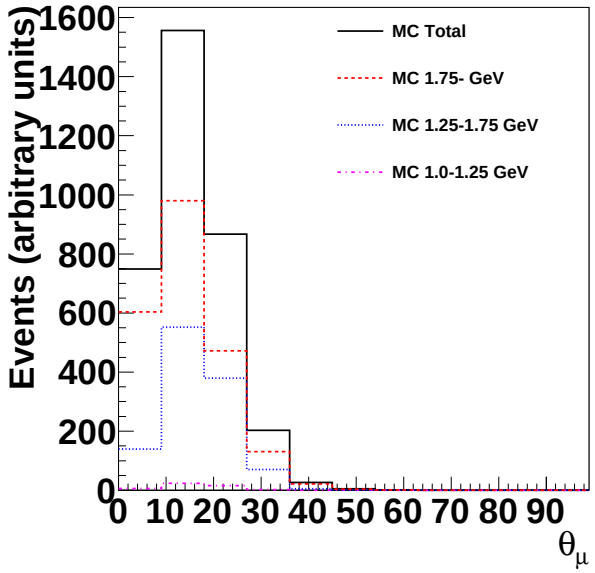

FIG. 13. (color online). The MC templates of θ_μ for the MRD-penetrated sample. The black line shows the total MC prediction. The predictions for $E_\nu > 1.75$ GeV, $1.25 < E_\nu < 1.75$ GeV and $1.0 < E_\nu < 1.25$ GeV are also shown.

TABLE X. Spectrum fit result for the NUANCE prediction. The first two rows are the best fit values and associated uncertainties. The subsequent columns and rows represent the correlation coefficients for each parameters.

	f_0	f_1	f_2	f_3	f_4	f_5
Best fit	1.650	1.312	1.359	1.378	1.360	0.898
Error	0.203	0.093	0.057	0.075	0.107	0.085
f_0	1.0000	0.2260	0.0716	-0.2470	-0.2916	0.0019
f_1	0.2260	1.0000	0.0244	-0.4319	-0.5275	-0.2410
f_2	0.0716	0.0244	1.0000	-0.2225	-0.1150	-0.3403
f_3	-0.2470	-0.4319	-0.2225	1.0000	0.0910	0.2003
f_4	-0.2916	-0.5275	-0.1150	0.0910	1.0000	-0.0569
f_5	0.0019	-0.2410	-0.3403	0.2003	-0.0569	1.0000

tributions. The errors on f_i obtained from the fit include the shape error from all the flux and the cross section uncertainties, and the absolute error from all the intranuclear interaction and detector response uncertainties, as they are included into the error matrix (V_{sys}). The errors shown in these plots are the quadrature sum of those constrained systematic errors and errors of the f_i. We find that both NEUT and NUANCE predictions well reproduce the data distributions within the errors of this analysis. Also, we confirm that the constraint by this measurement can reduce the systematic uncertainty in most regions, compared to the original errors.

The CC interaction rate in i-th true E_ν region, $\mathcal{R}_i$, is calculated as:

$$\mathcal{R}_i = \frac{f_i \cdot \mathcal{N}_i^{pred} \cdot P_i}{\epsilon_i}, \tag{10}$$

where $\mathcal{N}_i^{pred}$ is the number of selected events predicted by the MC simulation, P_i is the CC inclusive purity, and ϵ_i is the CC inclusive efficiency. We evaluate the errors on P_i/ϵ_i with all systematic uncertainties listed in Table VIII. Then we take the quadrature sum of the errors of f_i and P_i/ϵ_i to estimate the total systematic error. Figure 15 shows the obtained neutrino interaction rate normalized to the NEUT and NUANCE predictions, with the full systematic error. The original flux and cross-section uncertainties are also shown in the plot. The numerical values of the interaction rate normalized to the MC predictions and its full errors are shown in Table XI. The uncertainty is about 6% for the rate at $0.75 < E_\nu < 1.0$ GeV, where the CC interaction rate is maximum, and is about 15% for the lowest energy region.

TABLE XI. ν_μ CC inclusive interaction rate normalization factors to NEUT and NUANCE predictions. The size of the full systematic errors are also shown.

Energy region	ν_μ CC rate normalization factor	
(GeV)	NEUT	NUANCE
0.25 - 0.50	1.04 ± 0.20	1.65 ± 0.22
0.50 - 0.75	1.03 ± 0.11	1.31 ± 0.11
0.75 - 1.00	1.23 ± 0.08	1.36 ± 0.08
1.00 - 1.25	1.29 ± 0.10	1.38 ± 0.09
1.25 - 1.75	1.19 ± 0.11	1.36 ± 0.12
1.75 -	0.79 ± 0.08	0.90 ± 0.09

2. *CC Inclusive Cross Section*

The major difference between the rate normalization factors NEUT and NUANCE is (a) the difference in the predicted neutrino interaction cross sections of the two models. This effect is compensated by the rate normalization factor obtained by this analysis, and thus has little effect on the absolute rates.

However, there is also a second-order contribution to this difference from (b) the difference in the prediction of final state particle production and kinematics. This affects events with pion or proton tracks mis-reconstructed as muons, which ultimately affects the purity (P_i) and efficiency (ϵ_i) in Eq. (10).

To estimate the effect of (b), we extract the absolute CC interaction cross section from the obtained rate normalization factors. Here, the difference between NEUT and NUANCE due to (a) is canceled, and the remaining differences are, in principle, due to the source (b). The cross section per nucleon on polystyrene target (C_8H_8)

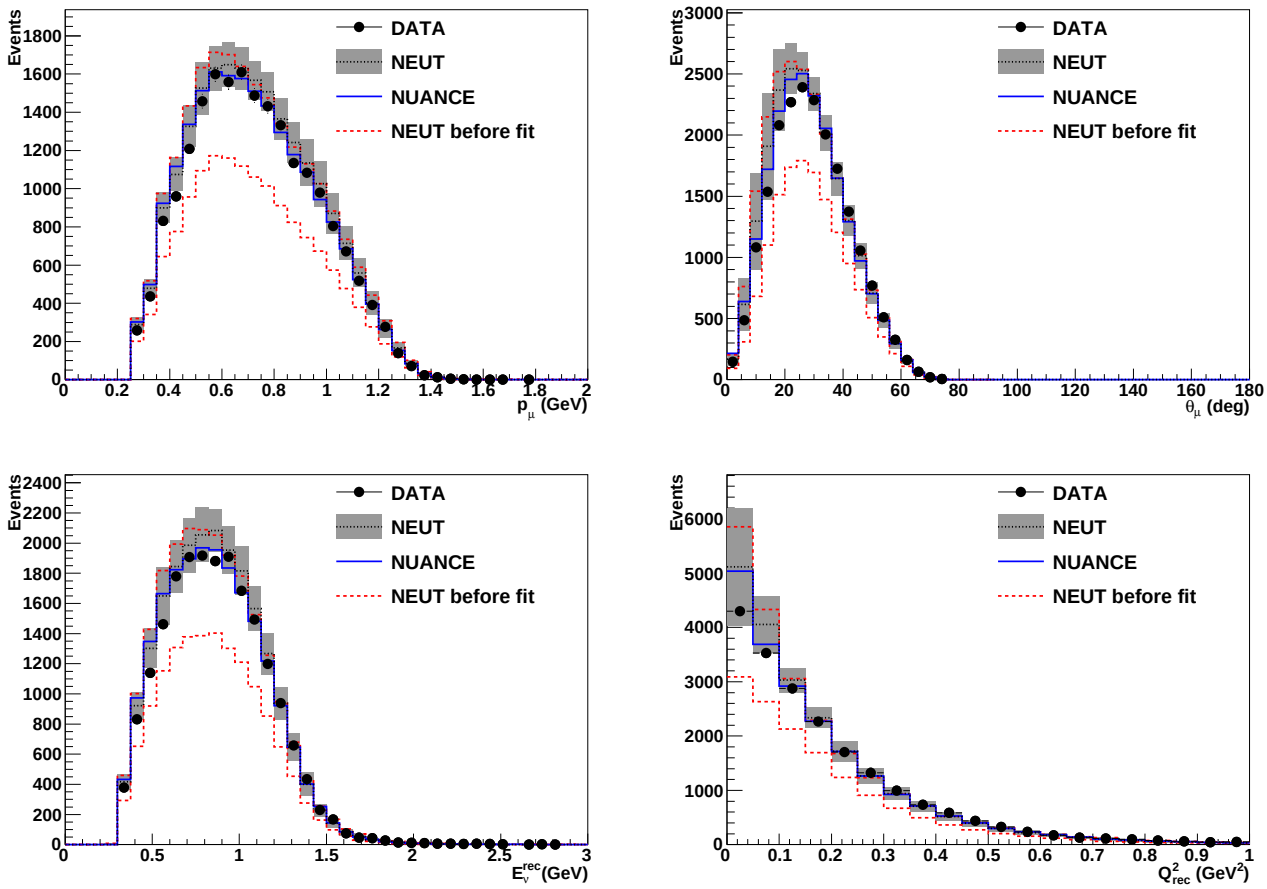

FIG. 14. (color online). Top: Reconstructed p_μ (left) and θ_μ (right) of the MRD-stopped sample. Bottom: E_ν^{rec} (left) and Q^2_{rec} (right) of the MRD-stopped sample. The NEUT and NUANCE predictions after the fit are shown, and the predictions are absolutely normalized by the number of POT. The filled regions show the systematic uncertainties of MC predictions based on NEUT. The area within dashed lines shows the NEUT predictions with their systematic uncertainties before the fit. The systematic uncertainty for the NUANCE prediction is similar to that of the NEUT prediction and not shown.

at each energy region is calculated as

$$\sigma_i = f_i \cdot < \sigma_{CC}^{pred} >_i = \frac{f_i \cdot \mathcal{N}_i^{pred} \cdot P_i}{\epsilon_i \cdot T \cdot \Phi_i}, \qquad (11)$$

where i is the index of the energy regions used for the spectrum fit (see Table VII), $< \sigma_{CC}^{pred} >_i$ is the predicted flux averaged CC interaction cross section per nucleon, $\mathcal{N}_i^{pred}$ is the number of selected events predicted by the MC simulation, P_i is the CC inclusive purity, ϵ_i is the CC inclusive efficiency, T_i is the number of nucleons in the SciBar fiducial volume, and Φ_i is the muon neutrino flux per unit area.

Figure 16 show the extracted cross sections plotted with the original predictions from NEUT and NUANCE. In addition to the errors on P_i/ϵ_i as estimated for the rate measurements, we also estimate the errors on Φ_i from the category (i) in the table. In the plot, we separately show the errors of f_i and the quadrature sum of f_i, P_i, ϵ_i and Φ_i errors. We confirm that the differences of the extracted CC interaction cross sections between NEUT and NUANCE are within the errors of f_i. Therefore, the effect of source (b) is small and covered by the systematic uncertainty. The difference of the rate normalization factors is mostly caused by the cross section difference itself (source (a)).

The obtained cross section values and their errors are summarized in Table XII. The uncertainty on the cross section is about 10% at $0.75 < E_\nu < 1.0$ GeV, where the CC interaction rate is maximum, and is about 30% for the lowest energy region.

B. Flux Integrated CC Interaction Rate

1. *Measurement of CC Interaction Rate*

We perform a fit with the method described in Sec. V using one rate normalization factor (f_{tot}) which spans the entire energy region, instead of six regions. This is motivated by the SciBooNE-MiniBooNE joint ν_μ disappear-

TABLE XII. Energy dependent CC inclusive cross section per nucleon on a polystyrene target (C_8H_8). Results based on NEUT and NUANCE based predictions are separately shown.

Energy region (GeV)	Mean Energy (GeV)	Total ν_μ flux (ν_μ/cm^2)	ν_μ CC inclusive cross section (cm^2/nucleon) NEUT based	NUANCE based
0.25 - 0.50	0.38	$(4.31 \pm 0.81) \times 10^{11}$	$(2.76 \pm 0.75) \times 10^{-39}$	$(3.40 \pm 0.96) \times 10^{-39}$
0.50 - 0.75	0.62	$(5.09 \pm 0.37) \times 10^{11}$	$(5.80 \pm 0.75) \times 10^{-39}$	$(6.39 \pm 0.81) \times 10^{-39}$
0.75 - 1.00	0.87	$(4.18 \pm 0.26) \times 10^{11}$	$(1.03 \pm 0.10) \times 10^{-38}$	$(1.01 \pm 0.09) \times 10^{-38}$
1.00 - 1.25	1.11	$(2.63 \pm 0.23) \times 10^{11}$	$(1.38 \pm 0.17) \times 10^{-38}$	$(1.29 \pm 0.15) \times 10^{-38}$
1.25 - 1.75	1.43	$(1.90 \pm 0.27) \times 10^{11}$	$(1.62 \pm 0.29) \times 10^{-38}$	$(1.56 \pm 0.28) \times 10^{-38}$
1.75 -	2.47	$(0.62 \pm 0.12) \times 10^{11}$	$(1.74 \pm 0.38) \times 10^{-38}$	$(1.66 \pm 0.37) \times 10^{-38}$

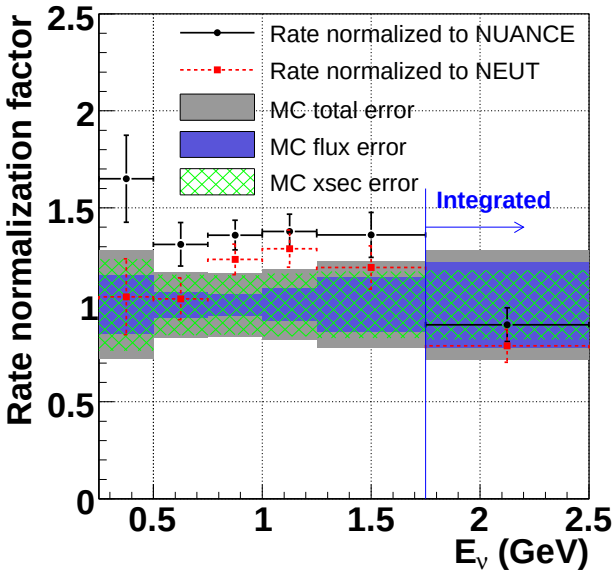

FIG. 15. (color online). CC interaction rate normalized to the NEUT and NUANCE predictions, obtained by the spectrum fit. The error bars show the full systematic uncertainties. The original flux and cross section errors are also shown separately.

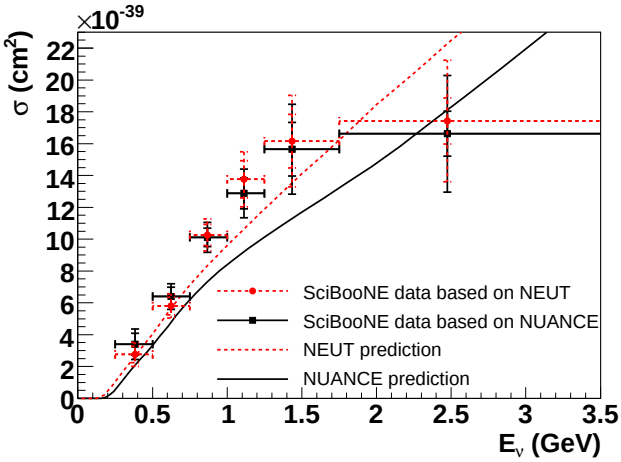

FIG. 16. (color online). CC inclusive interaction cross section per nucleon on a polystyrene target (C_8H_8). The smaller error bars show the uncertainties of the rate normalization factors, and the larger error bars represents the total error including the flux uncertainties.

ance analysis, in which we also evaluate the sensitivity using one rate normalization factor.

The obtained rate normalization factors are $1.12 \pm 0.02 \pm 0.03$, and $1.29 \pm 0.02 \pm 0.03$ for the NEUT and NUANCE predictions, respectively. The first errors show the errors from the fit, and the second show the errors from efficiency and purity uncertainties. Here, higher rate normalization factors compared to the simple ratio of the number of events (Table VI) are obtained. This is because the "shape" systematic uncertainty (Sec. V B) is calculated over the entire energy region, and it typically becomes smallest where the CC interaction rate is maximum. Hence, the obtained rate normalization factors tend to be close to the results for $0.75 < E_\nu < 1.0$ GeV in the energy dependent analysis (Sec. VI A). The χ^2/DOF, for NEUT and NUANCE predictions are respectively 208.6/159 and 481.5/159 before fitting, and they are 173.0/158 and 183.0/158 after fitting.

2. CC Inclusive Cross Section

We extract the total CC inclusive cross section for the flux at $E_\nu > 0.25$ GeV using a similar formula to Eq. (11):

$$\sigma = f_{tot} \cdot < \sigma_{CC}^{pred} >= \frac{f_{tot} \cdot \mathcal{N}^{pred} \cdot P}{\epsilon \cdot T \cdot \Phi}. \qquad (12)$$

The purity (P) and the efficiency (ϵ) are estimated for the sum of SciBar-stopped, MRD-stopped and MRD-penetrated samples, and obtained to be $P = 90.0(89.1)\%$ and $\epsilon = 34.5(34.5)\%$ with the NEUT(NUANCE) generators. The integrated ν_μ flux at $E_\nu > 0.25$ GeV averaged over the SciBar FV for 9.9E19 POT is estimated to be $\Phi = (1.87 \pm 0.14) \times 10^{12}$ (ν_μ/cm^2), with mean energy of 0.83 GeV.

Using these purity, efficiency and flux predictions, we obtain the total CC cross sections per nucleon on a polystyrene target for a muon neutrino beam

with mean energy of 0.83 GeV to be $(8.51 \pm 0.72) \times 10^{-39}$ cm^2/nucleon and $(8.45 \pm 0.71) \times 10^{-39}$ cm^2/nucleon for NEUT and NUANCE based predictions, respectively. The error contains all systematic uncertainties from the purity and efficiency variation and absolute flux uncertainty. The error is dominated by the uncertainty on the total flux prediction (7.6%). We obtain consistent CC interaction cross sections from the two neutrino generator simulations.

3. *CC Inclusive Cross Section for Previous SciBooNE Results*

In previous SciBooNE publications, the total CC interaction cross sections were used to normalize the results. We have used the number of MRD-matched and MRD-penetrated samples to extract the total CC cross section for CC coherent pion production measurements [15], and used MRD-stopped sample for NC neutral pion production measurements [16, 17]. We extract the absolute CC inclusive cross section from the number of each sub-sample as:

$$\sigma = \frac{\mathcal{N}^{obs} \cdot P}{\epsilon \cdot T \cdot \Phi}, \tag{13}$$

where $\mathcal{N}^{obs}$ is the observed number of events in each sub-sample, P is the purity of ν_μ CC interaction in the sample.

Table XIII is a summary of the absolute CC cross section extracted from the number of events in each sub-sample. Since we made minor improvements to the MC prediction and the reconstruction algorithms, the number of events in each sub-sample are slightly different from the previous published results. The difference in the number of events are included in the systematic uncertainties.

For the cross section values extracted from the MRD-matched and the MRD-stopped samples, the dominant source of uncertainty is the total flux (Φ) uncertainty (7.6%). The second largest uncertainty is the efficiency (ϵ) uncertainty due to the cross section models. They are 4.0% and 5.0% in the MRD-matched and the MRD-stopped samples, respectively.

For the MRD-penetrated sample, the dominant systematic error from the efficiency variation is due to the flux model uncertainties. Approximately 40% of the MRD-penetrated sample is from neutrinos from kaon decay, which have a large uncertainty, as shown in Fig. 2. The error from the efficiency variation due to the flux model is estimated to be 18.1%. The second largest error comes from the the total flux (Φ) uncertainty (7.6%).

With these cross section values, one can convert the cross section ratios of our previous results to absolute cross sections.

VII. CONCLUSIONS

In conclusion, we have isolated three ν_μ CC data samples, measured p_μ and θ_μ, and extracted the CC interaction rates and cross sections using flux and neutrino interaction simulations.

We extract the ν_μ CC interaction rates by fitting muon kinematics, with precision of 6-15% for the energy dependent and 3% for the energy integrated analyses. We confirm that the distributions after fitting well reproduce the observed distributions with both NEUT and NUANCE based simulations. This result will be used to constrain the neutrino interaction rate for a SciBooNE-MiniBooNE joint ν_μ disappearance analysis [13].

We also evaluate CC inclusive interaction cross sections, and the results are consistent with both NEUT and NUANCE predictions. This confirms that the difference in the observed rates normalized to the NEUT and NUANCE based predictions is mainly due to the cross section difference of the two simulators. The precisions of the obtained cross sections are 10-30% for energy dependent and 8% for the energy integrated analyses. This is the first measurement of the CC inclusive cross section on carbon around 1 GeV. The total CC interaction cross section values, as defined in our previous publications [15–17], are also extracted. These cross section values can be used to convert previous measurements of cross section ratios of exclusive channels at SciBooNE to the absolute scale. The results may also be used to tune neutrino interaction models in the $\sim$1 GeV region, which is relevant to various ongoing and future neutrino oscillation experiments.

VIII. ACKNOWLEDGMENTS

We acknowledge the Physics Department at Chonnam National University, Dongshin University, and Seoul National University for the loan of parts used in SciBar and the help in the assembly of SciBar. We wish to thank the Physics Departments at the University of Rochester and Kansas State University for the loan of Hamamatsu PMTs used in the MRD. We gratefully acknowledge support from Fermilab as well as various grants, contracts and fellowships from the MEXT and JSPS (Japan), the INFN (Italy), the Ministry of Science and Innovation and CSIC (Spain), the STFC (UK), and the DOE and NSF (USA). This work was supported by MEXT and JSPS with the Grant-in-Aid for Scientific Research A 19204026, Young Scientists S 20674004, Young Scientists B 18740145, Scientific Research on Priority Areas "New Developments of Flavor Physics", and the global COE program "The Next Generation of Physics, Spun from Universality and Emergence". The project was supported by the Japan/U.S. Cooperation Program in the field of High Energy Physics and by JSPS and NSF under the Japan-U.S. Cooperative Science Program.

TABLE XIII. Extracted number of total CC interaction and absolute cross sections per nucleon on a polystyrene target, based on the number of events in each sub-sample. The MC predictions are based on NEUT.

sample	Events ($\mathcal{N}^{obs}$)	Mean energy of selected sample [GeV]	Efficiency (ϵ)	Purity (P)	Total CC events ($\mathcal{N}^{obs}P/\epsilon$)	Flux integrated CC cross-section (σ [cm^2/nucleon])
MRD-match	28409.6	1.43	27.2%	92.9%	$(9.71 \pm 0.69) \times 10^4$	$(8.14 \pm 0.85) \times 10^{-39}$
MRD-stop	20236.4	1.20	18.5%	91.2%	$(10.0 \pm 0.73) \times 10^4$	$(8.34 \pm 0.88) \times 10^{-39}$
MRD-pene	3544.4	2.42	4.3%	97.1%	$(7.94 \pm 1.54) \times 10^4$	$(6.65 \pm 1.29) \times 10^{-39}$

[1] Q. Wu *et al.* (NOMAD), Phys. Lett. **B660**, 19 (2008), arXiv:0711.1183 [hep-ex].
[2] P. Adamson *et al.* (MINOS), Phys. Rev. D **81**, 072002 (2010), arXiv:0910.2201 [hep-ex].
[3] S. J. Barish *et al.*, Phys. Rev. D **19**, 2521 (1979).
[4] N. J. Baker *et al.*, Phys. Rev. D **25**, 617 (1982).
[5] A. A. Aguilar-Arevalo *et al.* (MiniBooNE), Phys. Rev. Lett. **98**, 231801 (2007), arXiv:0704.1500 [hep-ex].
[6] Y. Itow *et al.* (T2K), arXiv:hep-ex/0106019.
[7] Y. Hayato, Nucl. Phys. Proc. Suppl. **112**, 171 (2002).
[8] G. Mitsuka (Super-Kamiokande), J. Phys. Conf. Ser. **136**, 042017 (2008).
[9] D. Casper, Nucl. Phys. Proc. Suppl. **112**, 161 (2002), arXiv:hep-ph/0208030.
[10] Y. Fukuda *et al.* (Kamiokande), Phys. Lett. **B335**, 237 (1994).
[11] Y. Ashie *et al.* (Super-Kamiokande), Phys. Rev. D **71**, 112005 (2005), arXiv:hep-ex/0501064.
[12] M. H. Ahn *et al.* (K2K), Phys. Rev. D **74**, 072003 (2006), arXiv:hep-ex/0606032.
[13] Y. Nakajima (SciBooNE), arXiv:1010.5721 [hep-ex].
[14] A. A. Aguilar-Arevalo *et al.* (MiniBooNE), Phys. Rev. Lett. **103**, 061802 (2009), arXiv:0903.2465 [hep-ex].
[15] K. Hiraide *et al.* (SciBooNE), Phys. Rev. D **78**, 112004 (2008).
[16] Y. Kurimoto *et al.* (SciBooNE), Phys. Rev. D **81**, 033004 (2010), arXiv:0910.5768 [hep-ex].
[17] Y. Kurimoto *et al.* (SciBooNE), Phys. Rev. D **81**, 111102 (2010), arXiv:1005.0059 [hep-ex].
[18] S. Agostinelli *et al.* (GEANT4), Nucl. Instrum. Meth. **A506**, 250 (2003).
[19] M. G. Catanesi *et al.*, Eur. Phys. J. **C52**, 29 (2007), arXiv:hep-ex/0702024.
[20] I. Chemakin *et al.* (E910), Phys. Rev. C **77**, 015209 (2008), arXiv:0707.2375 [nucl-ex].
[21] A. A. Aguilar-Arevalo *et al.* (MiniBooNE), Phys. Rev. D **79**, 072002 (2009), arXiv:0806.1449 [hep-ex].
[22] K. Nitta *et al.*, Nucl. Instrum. Meth. **A535**, 147 (2004), arXiv:hep-ex/0406023.
[23] H. Maesaka, Ph.D. thesis, Kyoto University (2005).
[24] M. Yoshida *et al.*, IEEE Trans. Nucl. Sci. **51**, 3043 (2004).
[25] A. Heikkinen, N. Stepanov, and J. P. Wellisch, in *Proceedings of 2003 Conference for Computing in High-Energy and Nuclear Physics (CHEP 03), La Jolla, California, 24-28 Mar 2003* (2003) p. MOMT008, arXiv:nucl-th/0306008.
[26] M. Hasegawa, Ph.D. thesis, Kyoto University (2006).
[27] R. A. Smith and E. J. Moniz, Nucl. Phys. **B43**, 605 (1972).
[28] E. J. Moniz *et al.*, Phys. Rev. Lett. **26**, 445 (1971).
[29] A. A. Aguilar-Arevalo *et al.* (MiniBooNE), Phys. Rev. Lett. **100**, 032301 (2008), arXiv:0706.0926 [hep-ex].
[30] H. S. Budd, A. Bodek, and J. Arrington, arXiv:hep-ex/0308005.
[31] A. A. Aguilar-Arevalo *et al.* (MiniBooNE), Phys. Rev. D **81**, 092005 (2010), arXiv:1002.2680 [hep-ex].
[32] A. Bodek, S. Avvakumov, R. Bradford, and H. S. Budd, J. Phys. Conf. Ser. **110**, 082004 (2008), arXiv:0709.3538 [hep-ex].
[33] D. Rein and L. M. Sehgal, Ann. Phys. **133**, 79 (1981).
[34] D. Rein, Z. Phys. **C35**, 43 (1987).
[35] D. Rein and L. M. Sehgal, Nucl. Phys. **B223**, 29 (1983).
[36] D. Rein and L. M. Sehgal, Phys. Lett. **B657**, 207 (2007), arXiv:hep-ph/0606185.
[37] K. Nakamura *et al.* (Particle Data Group), J. Phys. **G37**, 075021 (2010).
[38] A. A. Aguilar-Arevalo *et al.* (MiniBooNE), Phys. Lett. **B664**, 41 (2008), arXiv:0803.3423 [hep-ex].
[39] M. Gluck, E. Reya, and A. Vogt, Eur. Phys. J. **C5**, 461 (1998), arXiv:hep-ph/9806404.
[40] A. Bodek and U. K. Yang, arXiv:hep-ex/0308007.
[41] M. Nakahata *et al.* (Kamiokande), J. Phys. Soc. Jap. **55**, 3786 (1986).
[42] T. Sjostrand, Comput. Phys. Commun. **82**, 74 (1994).
[43] D. Ashery *et al.*, Phys. Rev. C **23**, 2173 (1981); R. D. Ransome *et al.*, *ibid.* **45**, 509 (1992); M. K. Jones *et al.*, *ibid.* **48**, 2800 (1993).
[44] J. L. Alcaraz-Aunion, Ph.D. thesis, Universidad Autonoma de Barcelona (2010).